Journal of
Mechanics of
Materials and Structures

VISCOELASTIC STATE OF A SEMI-INFINITE MEDIUM WITH MULTIPLE CIRCULAR ELASTIC INHOMOGENEITIES

Andrey V. Pyatigorets and Sofia G. Mogilevskaya

VISCOELASTIC STATE OF A SEMI-INFINITE MEDIUM WITH MULTIPLE CIRCULAR ELASTIC INHOMOGENEITIES

ANDREY V. PYATIGORETS AND SOFIA G. MOGILEVSKAYA

This paper is concerned with the problem of an isotropic, linear viscoelastic half-plane containing multiple, isotropic, circular elastic inhomogeneities. Three types of loading conditions are allowed at the boundary of the half-plane: a point force, a force uniformly distributed over a segment, and a force uniformly distributed over the whole boundary of the half-plane. The half-plane is subjected to far-field stress that acts parallel to its boundary. The inhomogeneities are perfectly bonded to the material matrix. An inhomogeneity with zero elastic properties is treated as a hole; its boundary can be either traction free or subjected to uniform pressure. The analysis is based on the use of the elastic-viscoelastic correspondence principle. The problem in the Laplace space is reduced to the complementary problems for the bulk material of the perforated half-plane and the bulk material of each circular disc. Each problem is described by the transformed complex Somigliana's traction identity. The transformed complex boundary parameters at each circular boundary are approximated by a truncated complex Fourier series. Numerical inversion of the Laplace transform is used to obtain the time domain solutions everywhere in the half-plane and inside the inhomogeneities. The method allows one to adopt a variety of viscoelastic models. A number of numerical examples demonstrate the accuracy and efficiency of the method.

1. Introduction

The problem of an isotropic, linearly viscoelastic half-plane containing multiple, nonoverlapping circular inhomogeneities is of practical importance in the area of mechanics of composite materials. Analysis of the relevant literature reveals that the problem has not yet received significant attention.

Standard numerical methods such as the finite element method and the boundary element method can be used to solve the problems of viscoelastic media containing inhomogeneities. These methods require very fine meshes to adequately approximate the inhomogeneities or their boundaries and usually employ a time stepping procedure. In addition, the finite element method cannot directly model an infinite or semi-infinite area. As a result, these methods are computational intensive due to their large number of degrees of freedom.

There are few numerical methods custom designed to directly simulate the behavior of viscoelastic composite materials. The problem of an infinite, linear viscoelastic plane containing multiple, nonoverlapping, circular elastic inhomogeneities was considered in [Huang et al. 2005a] for the Kelvin viscoelastic model and in [Huang et al. 2005b] for the Boltzmann viscoelastic model. The numerical approach presented in these papers combines a direct boundary integral method, Fourier series approximations for the boundary unknowns, and a time-stepping algorithm. The method assumes a time-independent

viscoelastic Poisson's ratio. The same assumption was used by Zatula and Lavrenyuk [1995] and Kaminskii et al. [2002], who solved a system of boundary-temporal integral equations with the standard collocation boundary element method to model a viscoelastic half-plane containing circular or rectangular elastic inhomogeneities. The boundary conditions at the surface of the half-plane included a load distributed over a segment. Numerical results were presented for the case of one and two inhomogeneities only.

Kaloerov and Mironenko [2007] considered a linearly viscoelastic plate containing a row of aligned isotropic, elastic, elliptical inhomogeneities or cracks. The authors assumed that the bulk modulus of the plate is constant, while its Poisson's ratio at every moment in time t differs from the instantaneous value at $t = 0$ by a small parameter. Expanding the Kolosov–Muskhelishvili potentials for the problem in infinite series with respect to this parameter and equating the coefficients of the same powers of the parameter, the authors obtain the system of boundary conditions for the unknown functions. These functions themselves were represented by the infinite complex series. The coefficients in these series were determined by the least-squares method. The disadvantage of this technique is that the accuracy of this approach may depend on the choice of the small parameter.

The elastic problems of a piece-wise homogeneous half-plane containing multiple inhomogeneities have been studied extensively. A comprehensive review of the literature related to the elastic case is given by Legros et al. [2004] and Kushch et al. [2006].

This paper is concerned with the problem of an isotropic, linearly viscoelastic half-plane containing multiple, isotropic, circular elastic inhomogeneities. Three types of loading conditions are allowed at the boundary of the half-plane: a point force, a force uniformly distributed over a segment, and a force uniformly distributed over the whole boundary of the half-plane. The half-plane is subjected to far-field stress that acts parallel to its boundary. The analysis in the present paper is based on the use of the elastic-viscoelastic correspondence principle. The problem in Laplace space is reduced to the complementary problems for the bulk material of the perforated half-plane and the bulk material of each circular disc. Each problem is described by the transformed complex Somigliana's traction identity. The transformed complex boundary parameters at each circular boundary are approximated by a truncated complex Fourier series. Numerical inversion of the Laplace transform is used to obtain the time domain solutions everywhere in the half-plane and inside the inhomogeneities. The method does not assume a time-independent viscoelastic Poisson's ratio and allows one to adopt a variety of viscoelastic models. The method described in the present paper is an extension of [Pyatigorets et al. 2008], where the problem of an isotropic, linearly viscoelastic half-plane containing multiple holes was considered. The inversion of the Laplace transform in the latter problem could be performed analytically, which is not the case for the more general problem considered in the present paper.

The paper is organized as follows. After formulating the problem in Section 2, the system of governing boundary integral equations, written in the Laplace domain separately for each inhomogeneity and the viscoelastic matrix, is analyzed in Section 3. In Section 4, the approximations of the unknown displacements and tractions at the boundaries of the inhomogeneities are introduced. Using the Taylor series expansion method one arrives at the system of linear equations, where the vector of unknowns consists of the Fourier coefficients for the boundary parameters. The viscoelastic analogs of the Kolosov–Muskhelishvili potentials are used to obtain the displacements, strains, and stresses in the Laplace domain. The section concludes with a description of the procedure for the numerical inversion of the Laplace transform and discussion of the sources of errors. Three examples, presented in Section 5, show the

accuracy and effectiveness of the method. Two different constitutive models are used in the numerical modeling. The first example is aimed at comparing the results obtained by the present approach with those obtained by the finite element method. The second example investigates the influence of the elastic properties of the inhomogeneity on the behavior of the hoop stress at a point on its boundary. The third example studies the asymptotic behavior of stress state in the viscoelastic half-plane and inside the inhomogeneity for the case when the Burgers model is used to describe the shear response of the bulk material of the half-plane. Several closing remarks conclude the paper.

2. Problem formulation

Consider an isotropic, linearly viscoelastic half-plane ($y \leq 0$) containing an arbitrary number N of nonoverlapping, arbitrarily located, circular, isotropic elastic inhomogeneities, as shown in Figure 1a. The elastic properties of the inhomogeneities (shear moduli μ_k and Poisson's ratios ν_k, $k = 1, \ldots, N$) are assumed to be arbitrary. A hole is treated as a particular case of an inhomogeneity with zero elastic properties. Let R_k, z_k, and L_k denote the radius, the center, and the boundary of the k-th inhomogeneity.

Three types of loading conditions are allowed at the surface $y = 0$ of the half-plane. These loads are: a point force $F(t)$ applied at point a, a force $F(t)$ uniformly distributed over the segment (a, b), a force $F(t)$ uniformly distributed over the whole boundary of the half-plane. The far-field stress $\sigma^\infty(t)$ acts parallel to the boundary of the half-plane. Perfect bonding is assumed between each inhomogeneity and the bulk material of the half-plane. In the case of a hole, its boundary is assumed to be either traction free or subjected to uniform pressure $-p_k(t)$, $k = 1, \ldots, N_h$ (where N_h is the number of holes). For practical applications it is sufficient to assume the following time-dependent behavior for the functions $p_k(t)$, $F(t)$, and $\sigma^\infty(t)$:

$$p_k(t) = \widetilde{p}_k \cdot f_p(t), \quad k = 1, \ldots, N_h, \qquad F(t) = \widetilde{F} \cdot f_F(t), \qquad \sigma^\infty(t) = \widetilde{\sigma}^\infty \cdot f_\infty(t), \qquad (1)$$

where the constants $\widetilde{p}_k, \widetilde{\sigma}^\infty$ are real and the constant $\widetilde{F}$ is complex ($\widetilde{F} = \widetilde{F}_x + i\widetilde{F}_y, i = \sqrt{-1}$). The first expression from (1) implies similar time-dependent behavior for all the functions $p_k(t)$, the second expression implies that the time-dependent behavior of the normal and tangential components of the surface loads is similar, and the third expression is added for consistency.
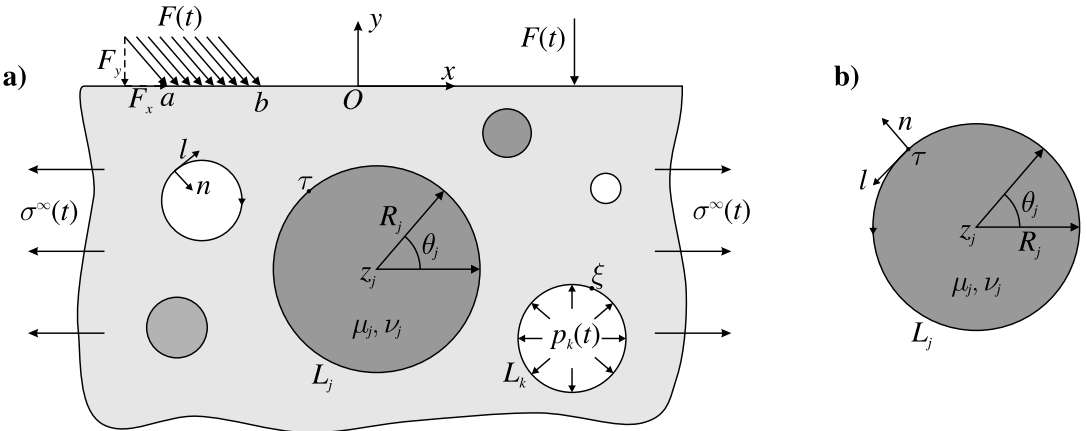

Figure 1. Problem formulation.

The viscoelastic model is not specified at this point, as the method enables the adoption of various models. The evolution of stresses, strains, and displacements in the viscoelastic half-plane and inside the inhomogeneities are to be determined.

3. Basic equations

The problem considered here can be decomposed into $N_d = N - N_h$ problems for each elastic disc and a complementary problem for the half-plane containing N cavities. The problems are interrelated by the condition of perfect bonding between the matrix and the discs.

The analysis is based on the elastic-viscoelastic correspondence principle. According to the principle, the solution of the problem in the time domain can be directly obtained from the solution of the corresponding elastic problem by applying the inverse Laplace transform to s-dependent quantities [Findley et al. 1976], where s is the transform parameter.

The Laplace transform of a real function $f(t)$ is defined as

$$\hat{f}(s) = \mathcal{L}[f(t)] = \int_0^\infty f(t)e^{-st}dt, \tag{2}$$

where s in general is a complex number. The inverse Laplace transform is given by the Bromwich integral

$$f(t) = \mathcal{L}^{-1}[\hat{f}(s)] = \frac{1}{2\pi i}\int_{\gamma - i\cdot\infty}^{\gamma + i\cdot\infty} \hat{f}(s)e^{st}ds, \tag{3}$$

where γ is a vertical contour in the complex plane to the right of all singularities of $\hat{f}(s)$.

3.1. *The system of boundary integral equations in the Laplace domain.* The system of governing equations in the Laplace domain is obtained by using a direct boundary integral method. This formulation is based on the use of the transformed Somigliana's displacement identity, which is a corollary of the reciprocal theorem (the principle of virtual work). The identity expresses the displacements at a point within an elastic region in terms of the integrals of the tractions and displacements over its boundary. Using the strain-displacement relation, Hooke's law, and the stress-traction relation, one can arrive then at the integral identity for the traction at the inner point of the region (Somigliana's traction identity). The tractions at the boundary of the region can be obtained through the limiting process in which the inner point of the region is allowed to approach the boundary of the region [Mogilevskaya and Linkov 1998; Mogilevskaya 2000]. Somigliana's identities can be written either in the time domain [Carini et al. 1991] or in the Laplace domain. In the following we use complex variable identities in the Laplace domain [Huang et al. 2006a]. Thus, the system of governing equations includes the following equations:

(I) The viscoelastic analog of Somigliana's traction identity at the boundary of the k-th disc, $k=1,\ldots,N_d$:

$$2\pi i \frac{\kappa_k + 1}{4\mu_k}\hat{\sigma}_k^d(\xi; s) = \frac{1 - \kappa_k}{2\mu_k}\int_{L_k}\hat{\sigma}_k^d(\tau; s)\frac{d\tau}{\tau - \xi} - \frac{\kappa_k}{2\mu_k}\int_{L_k}\hat{\sigma}_k^d(\tau; s)\frac{\partial}{\partial\xi}K_1(\tau, \xi)d\tau$$

$$+ \frac{1}{2\mu_k}\int_{L_k}\overline{\hat{\sigma}_k^d(\tau; s)}\frac{\partial}{\partial\xi}K_2(\tau, \xi)d\bar{\tau} + 2\int_{L_k}\frac{\hat{u}_k^d(\tau; s)}{(\tau - \xi)^2}d\tau$$

$$- \int_{L_k}\hat{u}_k^d(\tau; s)\frac{\partial^2}{\partial\tau\partial\xi}K_1(\tau, \xi)d\tau - \int_{L_k}\overline{\hat{u}_k^d(\tau; s)}\frac{\partial^2}{\partial\bar{\tau}\partial\xi}K_2(\tau, \xi)d\bar{\tau}. \tag{4}$$

Here $\xi = \xi_x + i\xi_y$, $\tau = \tau_x + i\tau_y$ are complex coordinates of the points $(\xi_x, \xi_y) \in L_k$ and $(\tau_x, \tau_y) \in L_k$; s is the Laplace transform parameter; $\hat{\sigma}_k^d(\tau; s) = \hat{\sigma}_{kn}^d(\tau; s) + i\hat{\sigma}_{kl}^d(\tau; s)$ is the unknown transformed complex traction at the point τ in the local coordinate system shown in Figure 1b; $\hat{u}_k^d(\tau; s) = \hat{u}_{kx}^d(\tau; s) + i\hat{u}_{ky}^d(\tau; s)$ is the unknown transformed complex displacement at the point τ in a global coordinate system; κ_k is the Kolosov–Muskhelishvili parameter for the k-th disc, equal to $3 - 4\nu_k$ for plane strain and to $(3 - \nu_k)/(1 + \nu_k)$ for plane stress; a bar over a symbol denotes complex conjugation; and a hat over a symbol denotes the transformed quantity (in the Laplace domain). The direction of travel is counterclockwise for the boundary L_k.

The kernels K_1 and K_2 in (4) corresponding to the Kelvin fundamental solution are [Mogilevskaya and Linkov 1998]

$$K_1(\tau, \xi) = \ln \frac{\tau - \xi}{\bar{\tau} - \bar{\xi}}, \qquad K_2(\tau, \xi) = \frac{\tau - \xi}{\bar{\tau} - \bar{\xi}}. \tag{5}$$

(II) The viscoelastic analog of Somigliana's traction identity at the boundary of the k-th cavity located in the viscoelastic half-plane, $k = 1, \ldots, N$,

$$\sum_{j=1}^{N} \left\{ 2 \int_{L_j} \frac{\hat{u}_j^h(\tau; s)}{(\tau - \xi)^2} d\tau - \int_{L_j} \hat{u}_j^h(\tau; s) \frac{\partial^2}{\partial \tau \partial \xi} [K_1(\tau, \xi) + K_3(\tau, \xi) + K_4(\tau, \xi)] d\tau \right.$$

$$\left. - \int_{L_j} \overline{\hat{u}_j^h(\tau; s)} \frac{\partial^2}{\partial \bar{\tau} \partial \xi} [K_2(\tau, \xi) + K_5(\tau, \xi) + K_6(\tau, \xi)] d\bar{\tau} \right\} - \pi i \frac{\hat{\kappa}(s) + 1}{2\hat{\mu}(s)} \hat{\sigma}_k^h(\xi; s)$$

$$- \frac{1}{2\hat{\mu}(s)} \sum_{j=1}^{N} \left\{ (\hat{\kappa}(s) - 1) \int_{L_j} \frac{\hat{\sigma}_j^h(\tau; s)}{\tau - \xi} d\tau + \int_{L_j} \hat{\sigma}_j^h(\tau; s) \frac{\partial}{\partial \xi} [\hat{\kappa}(s) K_1(\tau, \xi) + \hat{\kappa}(s) K_3(\tau, \xi) - K_4(\tau, \xi)] d\tau \right.$$

$$\left. - \int_{L_j} \overline{\hat{\sigma}_j^h(\tau; s)} \frac{\partial}{\partial \xi} [K_2(\tau, \xi) + K_6(\tau, \xi) - \hat{\kappa}(s) K_5(\tau, \xi)] d\bar{\tau} \right\} = -2\pi i \frac{\hat{\kappa}(s) + 1}{4\hat{\mu}(s)} \hat{\sigma}_k^{\mathrm{add}}(\xi; s), \quad (6)$$

where $\hat{u}_j^h(\tau; s) = \hat{u}_{jx}^h(\tau; s) + i\hat{u}_{jy}^h(\tau; s)$ is the unknown transformed complex displacement at the point $\tau \in L_j$, $\hat{\sigma}_j^h(\tau; s) = \hat{\sigma}_{jn}^h(\tau; s) + i\hat{\sigma}_{jl}^h(\tau; s)$ is the unknown transformed complex traction at the point $\tau \in L_j$ in the local coordinate system shown in Figure 1a, and $\hat{\kappa}(s)$ and $\hat{\mu}(s)$ are the transformed Kolosov–Muskhelishvili parameter and the shear modulus of the bulk material of the half-plane, respectively. The direction of travel is clockwise for the boundary L_j.

In addition to the kernels K_1 and K_2 from (5) the following kernels appear in system (6):

$$K_3(\tau, \xi) = \ln(\bar{\tau} - \xi), \qquad K_4(\tau, \xi) = \ln(\tau - \bar{\xi}) + (\xi - \bar{\xi}) \frac{\bar{\tau} - \tau}{(\tau - \bar{\xi})^2},$$

$$K_5(\tau, \xi) = \frac{\xi - \bar{\xi}}{\tau - \bar{\tau}}, \qquad K_6(\tau, \xi) = -\frac{\tau - \xi}{\bar{\tau} - \xi}. \tag{7}$$

The integral kernels K_3–K_6 are parts of Melan's fundamental solution [1932] (a point force applied at an internal point of a half-plane). Due to the use of this fundamental solution, the boundary of the half-plane is not involved in the governing system (6).

The function $\hat{\sigma}_k^{\mathrm{add}}(\xi; s)$ on the right-hand side of (6) is a complex function that represents the combined influence of the transformed far-field stress $\hat{\sigma}^\infty(s)$ and transformed force $\hat{F}(s)$ applied at the boundary

of the half-plane. It is expressed as

$$\hat{\sigma}_k^{\mathrm{add}}(\xi; s) = 2\hat{\sigma}_k^\infty(\xi; s) + \hat{\sigma}_k^F(\xi; s), \tag{8}$$

where $\hat{\sigma}_k^\infty(\xi; s)$ is the transformed traction at the trace of the boundary of the k-th cavity ($k = 1, \ldots, N$) due to the far-field stress and $\hat{\sigma}_k^F(\xi; s)$ is the transformed traction at the same boundary due to the force applied at the boundary of the half-plane. Both terms on the right-hand side of (8) are obtained by using s-varying Kolosov–Muskhelishvili potentials $\hat{\varphi}(\xi; s)$ and $\hat{\psi}(\xi; s)$ (see [Muskhelishvili 1959]) and the formula

$$\hat{\sigma}(\xi; s) = \frac{\partial}{\partial \xi}\hat{\varphi}(\xi; s) + \overline{\frac{\partial}{\partial \xi}\hat{\varphi}(\xi; s)} + \frac{d\bar{\xi}}{d\xi}\left[\overline{\xi\frac{\partial^2}{\partial \xi^2}\hat{\varphi}(\xi; s)} + \overline{\frac{\partial}{\partial \xi}\hat{\psi}(\xi; s)}\right] \tag{9}$$

(see [Rabotnov 1988]), where $d\bar{\xi}/d\xi = \exp(-2i\beta)$, and β is the angle between the axis Ox and the tangent at the point $\xi \in L_k$. The potentials $\hat{\varphi}$ and $\hat{\psi}$ for the far-field stress and the load applied at the boundary of the half-plane are given in [Pyatigorets et al. 2008].

Equations (5) and (6) are complemented by the following boundary conditions. For the case when the k-th inhomogeneity is a hole, the traction $\hat{\sigma}_k^h(\tau; s)$ in (6) is $\hat{\sigma}_k^h(\tau; s) = -\hat{p}_k(s)$. For the case when the k-th inhomogeneity is an elastic disc, the conditions for perfect bonding are

$$\begin{aligned}
\hat{u}_k^h(\xi; s) &= \hat{u}_k^d(\xi; s) = \hat{u}_k(\xi; s), \quad \xi \in L_k, \\
\hat{\sigma}_k^h(\xi; s) &= \hat{\sigma}_k^d(\xi; s) = \hat{\sigma}_k(\xi; s), \quad \xi \in L_k.
\end{aligned} \tag{10}$$

3.2. *Calculation of the s-dependent fields in the composite system.* The transformed stresses and displacements at any point in the viscoelastic half-plane and inside the elastic discs are obtained using the following analogs of the Kolosov–Muskhelishvili formulae:

$$\begin{cases}
2\hat{\mu}(s)\hat{u}(z; s) = \hat{\kappa}(s)\hat{\varphi}(z; s) - z\overline{\frac{\partial}{\partial z}\hat{\varphi}(z; s)} - \overline{\hat{\psi}(z; s)}, \\
\hat{\sigma}_{xx}(z; s) + \hat{\sigma}_{yy}(z; s) = 4\,\mathrm{Re}\left[\frac{\partial}{\partial z}\hat{\varphi}(z; s)\right], \\
\hat{\sigma}_{yy}(z; s) - \hat{\sigma}_{xx}(z; s) + 2i\hat{\sigma}_{xy}(z; s) = 2\left[\bar{z}\frac{\partial^2}{\partial z^2}\hat{\varphi}(z; s) + \frac{\partial}{\partial z}\hat{\psi}(z; s)\right].
\end{cases} \tag{11}$$

The strains are expressed through the stresses in the Laplace domain as

$$\begin{cases}
\hat{\varepsilon}_{xx} + \hat{\varepsilon}_{yy} = \frac{1 - 2\hat{v}}{2\hat{\mu}}(\hat{\sigma}_{xx} + \hat{\sigma}_{yy}), \\
\hat{\varepsilon}_{yy} - \hat{\varepsilon}_{xx} + 2i\hat{\varepsilon}_{xy} = \frac{1}{2\hat{\mu}}(\hat{\sigma}_{yy} - \hat{\sigma}_{xx} + 2i\hat{\sigma}_{xy}).
\end{cases} \tag{12}$$

The corresponding sets of material properties for the inhomogeneities and the matrix should be used in (11) and (12) for the evaluation of viscoelastic fields. The expressions for the potentials involved in (11) and (12) are:

(a) Potentials for the k-th elastic disc ($\hat{\mu}(s) = \mu_k$ and $\hat{\kappa}(s) = \kappa_k$):

$$\hat{\varphi}_k(z; s) = -\frac{1}{2\pi i(\kappa_k + 1)}\left[\int_{L_k}\hat{\sigma}_k^d(\tau; s)\ln(\tau - z)d\tau - 2\mu_k\int_{L_k}\frac{\hat{u}_k(\tau; s)}{\tau - z}d\tau\right],$$

$$\hat{\psi}_k(z; s) = -\frac{1}{2\pi i(\kappa_k + 1)}\left\{\left[\int_{L_k}\hat{\sigma}_k^d(\tau; s)\frac{\bar{\tau}d\tau}{\tau - z} + \kappa_k\int_{L_k}\overline{\hat{\sigma}_k^d(\tau; s)}\ln(\tau - z)d\bar{\tau}\right]\right.$$

$$\left. + 2\mu_k\left[\int_{L_k}\frac{\overline{\hat{u}_k(\tau; s)}}{\tau - z}d\tau - \int_{L_k}\frac{\hat{u}_k(\tau; s)}{\tau - z}d\bar{\tau} + \int_{L_k}\frac{\hat{u}_k(\tau; s)\bar{\tau}}{(\tau - z)^2}d\tau\right]\right\}. \tag{13}$$

Expressions (13) are obtained by Laplace transforming the corresponding elastic potentials given in [Mogilevskaya et al. 2008].

(b) Potentials for the bulk material of the viscoelastic half-plane:

$$\hat{\varphi}(z; s) = \hat{\varphi}_{\text{plane}}(z; s) + \hat{\varphi}_{\text{aux}}(z; s) + \hat{\varphi}_F(z; s),$$

$$\hat{\psi}(z; s) = \hat{\psi}_{\text{plane}}(z; s) + \hat{\psi}_{\text{aux}}(z; s) + \hat{\psi}_F(z; s), \tag{14}$$

where $\hat{\varphi}_{\text{plane}}(z;s)$ and $\hat{\psi}_{\text{plane}}(z;s)$ are the potentials due to Kelvin's fundamental solution and $\hat{\varphi}_{\text{aux}}(z;s)$ and $\hat{\psi}_{\text{aux}}(z; s)$ are additional potentials associated with the use of Green's functions specific for a half-plane problem. The potentials $\hat{\varphi}_F(z; s)$ and $\hat{\psi}_F(z; s)$ are given in [Pyatigorets et al. 2008] and the rest are obtained by applying the Laplace transform to their elastic analogs [Mogilevskaya 2000]:

$$\hat{\varphi}_{\text{plane}}(z; s) = -\frac{1}{2\pi i(\hat{\kappa}(s) + 1)}\sum_{j=1}^{N}\left[\int_{L_j}\hat{\sigma}_j^h(\tau; s)\ln(\tau - z)d\tau - 2\hat{\mu}(s)\int_{L_j}\frac{\hat{u}_j(\tau; s)}{\tau - z}d\tau\right] + \frac{\hat{\sigma}^\infty(s)}{4}z,$$

$$\hat{\psi}_{\text{plane}}(z; s) = -\frac{1}{2\pi i(\hat{\kappa}(s) + 1)}\sum_{j=1}^{N}\left\{\left[\int_{L_j}\hat{\sigma}_j^h(\tau; s)\frac{\bar{\tau}d\tau}{\tau - z} + \hat{\kappa}(s)\int_{L_j}\overline{\hat{\sigma}_j^h(\tau; s)}\ln(\tau - z)d\bar{\tau}\right]\right. \tag{15}$$

$$\left. + 2\hat{\mu}(s)\left[\int_{L_j}\frac{\overline{\hat{u}_j(\tau; s)}}{\tau - z}d\tau - \int_{L_j}\frac{\hat{u}_j(\tau; s)}{\tau - z}d\bar{\tau} + \int_{L_j}\frac{\hat{u}_j(\tau; s)\bar{\tau}}{(\tau - z)^2}d\tau\right]\right\} - \frac{\hat{\sigma}^\infty(s)}{2}z,$$

$$\hat{\varphi}_{\text{aux}}(z; s) = -\frac{1}{2\pi i(\hat{\kappa}(s) + 1)}\sum_{j=1}^{N}\left\{\left[\hat{\kappa}(s)\int_{L_j}\hat{\sigma}_j^h(\tau; s)\ln(\bar{\tau} - z)d\tau + \int_{L_j}\overline{\hat{\sigma}_j^h(\tau; s)}\frac{\tau - z}{\bar{\tau} - z}d\bar{\tau}\right]\right.$$

$$\left. + 2\hat{\mu}(s)\left[\int_{L_j}\frac{\hat{u}_j(\tau; s)}{\bar{\tau} - z}d\bar{\tau} - \int_{L_j}\overline{\hat{u}_j(\tau; s)}d\frac{\tau - z}{\bar{\tau} - z}\right]\right\},$$

$$\hat{\psi}_{\text{aux}}(z; s) = -\frac{1}{2\pi i(\hat{\kappa}(s) + 1)}\sum_{j=1}^{N}\left\{z\left[\hat{\kappa}(s)\int_{L_j}\hat{\sigma}_j^h(\tau; s)\frac{d\tau}{\bar{\tau} - z} - \int_{L_j}\overline{\hat{\sigma}_j^h(\tau; s)}\frac{\partial}{\partial z}\frac{\tau - z}{\bar{\tau} - z}d\bar{\tau}\right.\right. \tag{16}$$

$$\left. + 2\hat{\mu}(s)\left(\int_{L_j}\overline{\hat{u}_j(\tau; s)}d\frac{\partial}{\partial z}\frac{\tau - z}{\bar{\tau} - z} - \int_{L_j}\hat{u}_j(\tau; s)\frac{d\bar{\tau}}{(\bar{\tau} - z)^2}\right)\right]$$

$$\left. + \int_{L_j}\overline{\hat{\sigma}_j^h(\tau; s)}\ln(\bar{\tau} - z)d\bar{\tau} - 2\hat{\mu}(s)\int_{L_j}\frac{\overline{\hat{u}_j(\tau; s)}}{\bar{\tau} - z}d\bar{\tau}\right\}.$$

4. Numerical solution

4.1. *Fourier series approximation of the unknowns at the boundaries.* The unknown transformed stresses $\hat{\sigma}_k(\tau; s)$ at each boundary L_k are approximated by the truncated complex Fourier series

$$\hat{\sigma}_k(\tau; s) = \sum_{m=1}^{M_k} \hat{T}_{-mk}(s) g_k^m(\tau) + \hat{T}_{0k}(s) + \sum_{m=1}^{M_k} \hat{T}_{mk}(s) g_k^{-m}(\tau), \quad \tau \in L_k, \quad k = 1, \ldots, N_d, \tag{17}$$

where the function $g_k(\tau)$ is defined as

$$g_k(\tau) = \frac{R_k}{\tau - z_k} = \exp(-i\theta_k). \tag{18}$$

The unknown transformed displacements $\hat{u}_k(\tau; s)$ at the boundary L_k are represented by the series

$$\hat{u}_k(\tau; s) = \sum_{m=1}^{M_k-1} \hat{B}_{-mk}(s) g_k^m(\tau) + \hat{B}_{0k}(s) + \sum_{m=1}^{M_k+1} \hat{B}_{mk}(s) g_k^{-m}(\tau), \quad \tau \in L_k, \quad k = 1, \ldots, N. \tag{19}$$

Note that the Fourier series in (19) are truncated differently from the series representation (17). The reason for this is explained in [Mogilevskaya et al. 2008].

4.2. *System of complex algebraic equations.* After substituting (17) and (19) into Somigliana's traction identity (4) and following a procedure similar to the one described in [Mogilevskaya et al. 2008] for the elastic case, one arrives at the expressions

$$\begin{aligned} \hat{T}_{-1k}(s) &= 0, \\ \frac{\kappa_k - 1}{2\mu_k} \hat{T}_{0k}(s) &= \frac{2}{R_k} \operatorname{Re} \hat{B}_{1k}(s), \\ \frac{1}{2\mu_k} \hat{T}_{-mk}(s) &= \frac{m-1}{R_k} \hat{B}_{-(m-1)k}(s), \quad m \geq 2, \\ \frac{\kappa_k}{2\mu_k} \hat{T}_{mk}(s) &= \frac{m+1}{R_k} \hat{B}_{(m+1)k}(s), \quad m \geq 1. \end{aligned} \tag{20}$$

Expression (17) can now be rewritten using (20) as

$$\hat{\sigma}_k(\tau; s) = \frac{2\mu_k}{R_k} \left[\sum_{m=1}^{M_k-1} m \hat{B}_{-mk}(s) g_k^{m+1}(\tau) + \frac{2}{\kappa_k - 1} \operatorname{Re} \hat{B}_{1k}(s) + \frac{1}{\kappa_k} \sum_{m=2}^{M_k+1} m \hat{B}_{mk}(s) g_k^{1-m}(\tau) \right],$$
$$k = 1, \ldots, N_d. \tag{21}$$

After substituting (19) and (21) in Somigliana's traction identity (6), the s-dependent Fourier coefficients $\hat{B}_{mk}(s)$ can be taken out from the integrals, and all the space integrals can be evaluated analytically.

As a result, one arrives at the following system of complex integral equations:

$$\hat{\Lambda}_{kk}(\xi; s) + \sum_{\substack{j=1 \\ j \neq k}}^{N_h} \hat{\Lambda}_{kj}(\xi; s) + \sum_{r=N_h+1}^{N} \hat{G}_{kr}(\xi; s) = -\frac{\hat{\kappa}+1}{4\hat{\mu}} \left(\hat{p}_k + \hat{\sigma}_k^{\text{add}}(\xi; s) \right) + \sum_{j=1}^{N_h} \hat{p}_j \hat{\Gamma}_j(\xi; s),$$

$$\xi \in L_k, \ k = 1, \dots, N_h,$$
$$(22)$$

$$\sum_{j=1}^{N_h} \hat{\Lambda}_{lj}(\xi; s) + \left[\hat{G}_{ll}(\xi; s) - \frac{\hat{\kappa}+1}{2\hat{\mu}} \hat{\sigma}_l(\xi; s) \right] + \sum_{\substack{r=N_h+1 \\ r \neq l}}^{N} \hat{G}_{lr}(\xi; s) = -\frac{\hat{\kappa}+1}{4\hat{\mu}} \hat{\sigma}_l^{\text{add}}(\xi; s) + \sum_{j=1}^{N_h} \hat{p}_j \hat{\Gamma}_j(\xi; s),$$

$$\xi \in L_l, \ l = N_h + 1, \dots, N.$$

The left-hand sides of (22) contain the unknown displacements at the boundaries of the cavities, while the right-hand sides contain the known boundary tractions only. The following operators appear in (22):

- operators $\hat{\Lambda}_{kj}(\xi; s)$ $(k, j = 1, \dots, N_h)$ obtained after evaluation of the integrals in (6) containing the unknown Fourier coefficients over the boundaries of the holes;
- operators $\hat{G}_{kj}(\xi; s)$ $(k, j = N_h, \dots, N)$ obtained after evaluation of the integrals in (6) containing the unknown Fourier coefficients over the boundaries of those cavities that later are occupied by the elastic discs;
- operators $\hat{\Gamma}_j(\xi; s)$ $(j = 1, \dots, N_h)$ obtained after evaluation of the integrals in (6) containing the known tractions $\hat{p}_j$ over the boundaries of the holes ($\hat{p}_j$ is factored out in (22)).

The coefficients $\hat{B}_{0k}(s)$ and the imaginary part of $\hat{B}_{1k}(s)$ are not involved in the system of governing equations (22). These coefficients are responsible for the rigid body translation (B_{0k}) and rotation (Im B_{1k}) and can be found from a procedure described in [Wang et al. 2003].

The expressions for the operators $\hat{\Lambda}_{\alpha\beta}$ and $\hat{\Gamma}_j$ can be obtained by applying the Laplace transform to the corresponding expressions used in [Dejoie et al. 2006]. Operators $\hat{G}_{\alpha\beta}$ differ from the expressions for $\hat{\Lambda}_{\alpha\beta}$ by additional s-dependent multipliers in front of the unknown coefficients $\hat{B}_{-mk}(s)$, Re $\hat{B}_{1k}(s)$, and $\hat{B}_{mk}(s)$ $(m = -(M_k - 1), \dots, M_k + 1, k = N_h + 1, \dots, N$; see Appendix A). These multipliers are

$$\hat{\alpha}_{1k} = -\left(\frac{\mu_k}{\hat{\mu}} - 1 \right) \qquad \text{in front of } \hat{B}_{-mk}(s),$$

$$\hat{\alpha}_{2k} = -\left(\frac{\mu_k}{\kappa_k - 1} \frac{\hat{\kappa}-1}{\hat{\mu}} - 1 \right) \quad \text{in front of Re } \hat{B}_{1k}(s), \qquad (23)$$

$$\hat{\alpha}_{3k} = -\left(\frac{\mu_k}{\kappa_k} \frac{\hat{\kappa}}{\hat{\mu}} - 1 \right) \qquad \text{in front of } \hat{B}_{mk}(s).$$

4.3. *System of real linear algebraic equations.* The Taylor expansion method (the so-called addition theorem) described in [Wang et al. 2003] can be used to obtain a system of linear algebraic equations from (22). In this method, all the functions $g_j^m(\xi)$ involved in the representations of the unknowns at the j-th boundary can be reexpanded in terms of infinite series of functions $g_k(\xi)$ as

$$g_j^m(\xi) = g_j^m(z_k) \sum_{q=0}^{\infty} \binom{m+q-1}{q} g_k^q(z_j) g_k^{-q}(\xi) \quad \text{for all } j \neq k \text{ and } j, k = 1, \dots, N, \qquad (24)$$

where $\binom{m+q-1}{q}$ represents a binomial coefficient as usual. The functions $\overline{g_j(\xi)}$ can similarly be reexpanded in terms of functions $g_k(\xi)$ due to the fact that

$$\overline{g_j(\xi)} = g_j^{-1}(\xi).$$

As a result, all the operators $\hat{\Lambda}_{\alpha\beta}$ and $\hat{G}_{\alpha\beta}$ in the left-hand side of (22) are expressed through the functions $g_k^q(\xi)$. Similarly, the operators $\hat{\Gamma}_j$ in the right-hand side of (22) can be expressed through the same functions. Using the orthogonality properties of the complex Fourier series, one can equate the coefficients in front of the terms $g_k^q(\xi)$ with the same powers in both sides of the obtained expressions. A finite system of linear equations with the number of equations equal to the number of unknown coefficients $\hat{B}_{mk}$, $k = 1, \ldots, N$, is obtained if one neglects the terms with powers $q > M_k$ and $q < -M_k$ in the Taylor series for every k.

As a result, one arrives at a system of $\sum_{k=1}^{N}(2M_k + 1)$ complex linear equations in the Laplace domain; namely, for $k = 1, \ldots, N$, we can write

$$\hat{\Upsilon}_{kk,q}(\hat{\mathbb{B}}_{mk}) + \sum_{\substack{j=1 \\ j \neq k}}^{N} \hat{\Upsilon}_{kj,q}(\hat{\mathbb{B}}_{mj}) + \Delta_k \cdot \hat{\Im}_k(\hat{\mathbb{B}}_{qk})$$

$$= \begin{cases} -\dfrac{\hat{\kappa}+1}{4\hat{\mu}}\hat{\sigma}^\infty - \dfrac{1-\Delta_k}{\hat{\mu}}\hat{p}_k - \dfrac{\hat{\kappa}+1}{4\hat{\mu}}\Omega_{k,0}(\hat{F}) + \dfrac{\hat{\kappa}-1}{2\hat{\mu}}\sum_{j=1}^{N_h}\hat{p}_j\,\Xi_{kj,0}, & \text{for } q=0, \\[3mm] -\dfrac{\hat{\kappa}+1}{4\hat{\mu}}\hat{\sigma}^\infty - \dfrac{\hat{\kappa}+1}{4\hat{\mu}}\Omega_{k,2}(\hat{F}) + \dfrac{\hat{\kappa}-1}{2\hat{\mu}}\sum_{j=1}^{N_h}\hat{p}_j\,\Xi_{kj,2}, & \text{for } q=2, \\[3mm] -\dfrac{\hat{\kappa}+1}{4\hat{\mu}}\Omega_{k,q}(\hat{F}) + \dfrac{\hat{\kappa}-1}{2\hat{\mu}}\sum_{j=1}^{N_h}\hat{p}_j\,\Xi_{kj,q}, & \text{for } q \neq 0,1,2,\ -M_k \leq q \leq M_k, \end{cases} \tag{25}$$

where

$$\hat{\Im}_k(\hat{\mathbb{B}}_{qk}) = \frac{\hat{\kappa}+1}{\hat{\mu}}\frac{\mu_k}{R_k} \cdot \begin{cases} \dfrac{1-q}{\hat{\alpha}_{3k}\kappa_k}\hat{\mathbb{B}}_{(1-q)k}, & \text{if } q \leq -1, \\[3mm] \dfrac{2}{\hat{\alpha}_{2k}(\kappa_k-1)}\,\mathrm{Re}\,\hat{\mathbb{B}}_{1k}, & \text{if } q = 0, \\[3mm] \dfrac{q-1}{\hat{\alpha}_{1k}}\hat{\mathbb{B}}_{(1-q)k}, & \text{if } q \geq 2, \end{cases} \tag{26}$$

and Δ_k takes the value 0 if L_k is the boundary of a hole and the value 1 if L_k is the boundary of a cavity later occupied by an elastic disc. In general, the coefficients $\hat{\mathbb{B}}_{mk}$ are different from the coefficients $\hat{B}_{mk}$ as they may include the multipliers given by (23). The operators $\hat{\Upsilon}_{kk,q}$, $\hat{\Upsilon}_{kj,q}$, $\Omega_{k,q}$, and $\Xi_{kj,q}$ can be found in [Pyatigorets et al. 2008][1] if one takes into account the specific method of truncating Fourier series in the present approach.

Separating the real and imaginary parts in complex equations (25) and taking into account that (25) is real for $q = 0$, one arrives at a linear system of $\sum_{k=1}^{N}(4M_k - 1)$ equations. The resulting system of linear equations can be written in matrix form as

$$\left[A + \hat{W}(s)\right] \cdot \hat{\mathbb{B}}(s) = \hat{D}(s), \tag{27}$$

---

[1]Due to misprints, all inequalities $q \leq -1$ present in [Pyatigorets et al. 2008, appendices A–C] should be read as $(-q) \leq -1$.

where the s-independent matrix A is

$$
A = \left[
\begin{array}{ccc|ccc}
\multicolumn{3}{c|}{\overbrace{\hspace{3cm}}^{\text{block 1}}} & \multicolumn{3}{c}{\overbrace{\hspace{4cm}}^{\text{block 2}}} \\
A_{11} & \cdots & A_{1N_h} & A_{1(N_h+1)} & \cdots & A_{1(N_h+N_d)} \\
\vdots & \ddots & \vdots & \vdots & \ddots & \vdots \\
A_{N_h1} & \cdots & A_{N_hN_h} & A_{N_h(N_h+1)} & \cdots & A_{N_h(N_h+N_d)} \\
\hline
A_{(N_h+1)1} & \cdots & A_{1N_h} & A_{(N_h+1)(N_h+1)} & \cdots & A_{(N_h+1)(N_h+N_d)} \\
\vdots & \ddots & \vdots & \vdots & \ddots & \vdots \\
A_{(N_h+N_d)1} & \cdots & A_{(N_h+N_d)N_h} & A_{(N_h+N_d)(N_h+N_d)} & \cdots & A_{(N_h+N_d)(N_h+N_d)} \\
\multicolumn{3}{c|}{\underbrace{\hspace{3cm}}_{\text{block 3}}} & \multicolumn{3}{c}{\underbrace{\hspace{4cm}}_{\text{block 4}}}
\end{array}
\right] . \tag{28}
$$

The matrix A consists of four blocks:

- block 1, the influence of a hole on another hole;
- block 2, the influence of a hole on a cavity occupied by an elastic disc;
- block 3, the influence of a cavity occupied by an elastic disc on a hole;
- block 4, the influence of a cavity occupied by an elastic disc on another cavity occupied by an elastic disc.

The expressions for submatrices A_{jk} are available in [Pyatigorets et al. 2008] if one takes into account the differing truncation of Fourier series in the present approach. The matrix $\hat{W}(s)$ is deduced from the expression for the operator $\hat{\mathfrak{I}}_k$. This matrix is largely sparse and has the form

$$
\hat{W}(s) = \left[
\begin{array}{ccc|ccc}
0 & \cdots & 0 & 0 & \cdots & 0 \\
\vdots & \ddots & \vdots & \vdots & \ddots & \vdots \\
0 & \cdots & 0 & 0 & \cdots & 0 \\
\hline
0 & \cdots & 0 & \hat{W}_{(N_h+1)(N_h+1)} & \cdots & 0 \\
\vdots & \ddots & \vdots & \vdots & \ddots & \vdots \\
0 & \cdots & 0 & 0 & \cdots & \hat{W}_{NN}
\end{array}
\right] , \tag{29}
$$

where the only nonzero submatrices $\hat{W}_{kk}(s)$ are of dimension $(4M_k - 1) \times (4M_k - 1)$, $k = N_h + 1, \ldots, N$. They have the form

$$
\hat{W}_{kk}(s) = -\frac{\hat{\kappa}+1}{\hat{\mu}} \frac{\mu_k}{R_k} \cdot \left[
\begin{array}{c|c|c}
\dfrac{q-1}{\alpha_{1k}} & 0 & 0 \\
\hline
0 & \dfrac{2}{\alpha_{2k}(\kappa_k-1)} & 0 \\
\hline
0 & 0 & \dfrac{q+1}{\alpha_{3k}\kappa_k}
\end{array}
\right] . \tag{30}
$$

The vector of unknowns $\hat{\mathbb{B}}(s)$ is given as

$$
\hat{\mathbb{B}}(s) = \begin{bmatrix} \hat{\mathbb{B}}_1(s) \\ \vdots \\ \hat{\mathbb{B}}_{N_h}(s) \\ \hline \hat{\mathbb{B}}_{N_h+1}(s) \\ \vdots \\ \hat{\mathbb{B}}_N(s) \end{bmatrix},
\tag{31}
$$

with the subvectors $\hat{\mathbb{B}}_k(s)$ defined as

$$
\hat{\mathbb{B}}_k(s) = \hat{B}_k(s) = \begin{bmatrix} \mathrm{Re}\,\hat{B}_{-(M_k-1)k} \\ \mathrm{Im}\,\hat{B}_{-(M_k-1)k} \\ \vdots \\ \mathrm{Re}\,\hat{B}_{-1k} \\ \mathrm{Im}\,\hat{B}_{-1k} \\ \mathrm{Re}\,\hat{B}_{1k} \\ \mathrm{Re}\,\hat{B}_{2k} \\ \mathrm{Im}\,\hat{B}_{2k} \\ \vdots \\ \mathrm{Re}\,\hat{B}_{(M_k+1)k} \\ \mathrm{Im}\,\hat{B}_{(M_k+1)k} \end{bmatrix}, \qquad
\hat{\mathbb{B}}_j(s) = \begin{bmatrix} \hat{\alpha}_{1j}\cdot\mathrm{Re}\,\hat{B}_{-(M_j-1)j} \\ \hat{\alpha}_{1j}\cdot\mathrm{Im}\,\hat{B}_{-(M_j-1)j} \\ \vdots \\ \hat{\alpha}_{1j}\cdot\mathrm{Re}\,\hat{B}_{-1j} \\ \hat{\alpha}_{1j}\cdot\mathrm{Im}\,\hat{B}_{-1j} \\ \hat{\alpha}_{2j}\cdot\mathrm{Re}\,\hat{B}_{1j} \\ \hat{\alpha}_{3j}\cdot\mathrm{Re}\,\hat{B}_{2j} \\ \hat{\alpha}_{3j}\cdot\mathrm{Im}\,\hat{B}_{2j} \\ \vdots \\ \hat{\alpha}_{3j}\cdot\mathrm{Re}\,\hat{B}_{(M_j+1)j} \\ \hat{\alpha}_{3j}\cdot\mathrm{Im}\,\hat{B}_{(M_j+1)j} \end{bmatrix},
\tag{32}
$$

where $k = 1, \ldots, N_h$ and $j = N_h + 1, \ldots, N$.

The right-hand vector in (27) can be deduced from the expressions for the operators $\Omega_{k,q}$ and $\Xi_{kj,q}$ in [Pyatigorets et al. 2008]. It contains N subvectors consisting of $4M_k - 1$, $k = 1, \ldots, N$, elements, and its transpose is

$$
\left[\hat{D}(s)\right]^{\mathsf{T}} = \left[\hat{D}_1(s),\, \hat{D}_2(s),\, \ldots,\, \hat{D}_{N_h}(s),\, \hat{D}_{N_h+1}(s),\, \ldots,\, \hat{D}_N(s)\right].
\tag{33}
$$

4.4. *Solution in the time domain.*

An algorithm for the numerical inversion of the Laplace transform. After the solution of system (27), the potentials involved in expressions (11) and (12) can be written in terms of s-dependent coefficients. Thus, the transformed fields can be expressed explicitly via the coefficients. To obtain the viscoelastic fields in the time domain, one needs to apply the inverse Laplace transform to the s-dependent terms involved in the transformed fields.

In the general case, the system (27) cannot be solved analytically as its both sides depend on the transform parameter s. This fact suggests that a procedure for numerical inversion of the Laplace transform should be used. Most of the methods of numerical Laplace inversion are based on the approximation of the integral (3) by a sum of s-dependent functions evaluated at certain points and multiplied by coefficients specific to a given point. For reviews of some popular methods, see [Davies and Martin 1979; Cheng et al. 1994].

Here we used the numerical Laplace inversion method proposed in [Stehfest 1970]. The series approximation for the Stehfest algorithm is given by

$$f(t) \approx \frac{\ln 2}{t} \sum_{n=1}^{N_{St}} C_n \hat{f}\left(n \frac{\ln 2}{t}\right), \tag{34}$$

where N_{St} is even and the coefficients C_n are

$$C_n = (-1)^{n+N_{St}/2} \sum_{k=(n+1)/2}^{\min(n,N_{St}/2)} \frac{k^{N_{St}/2}(2k)!}{(N_{St}/2-k)!\,k!\,(k-1)!\,(n-k)!\,(2k-n)!}. \tag{35}$$

The detailed derivation of expressions (34) and (35) can be found in [Stehfest 1970; Kumar 2000]. The number of terms N_{St} in the series is relatively small and usually varies in the range $2 \leq N_{St} \leq 20$ that makes the calculation procedure fast in comparison with some other methods; see the charts in [Davies and Martin 1979]. Due to its simplicity the algorithm can be easily implemented in various programming languages. In addition, the algorithm does not require knowledge of the poles of the integrand (see (3)). For the case of monotonic smooth functions quite accurate results are reported by Davies and Martin [1979], Cheng et al. [1994], and Stehfest [1970]. However, no accurate results of the inversion should be expected for discontinuous functions or functions containing sharp peaks or rapid oscillations.

As the number of terms in approximation (34) does not change during the calculation of viscoelastic fields, the coefficients C_n are evaluated only once and stored in the computer memory.

Calculation of viscoelastic fields in the time domain. In order to find the viscoelastic potentials in the time domain, one has to solve system (27) for each moment of time t and each point n in the Stehfest algorithm in accordance with expression (34). The Gauss–Seidel iterative algorithm combined with an algorithm based on LU decomposition is adopted to find the explicit solution of system (27). This technique provides a good convergence rate even if the dimension of matrix A is very large. After that all s-dependent terms involved in potentials (13)–(16) have to be evaluated at points $(n \ln 2/t)$. The expressions for the potentials in terms of the Fourier coefficients $\hat{\mathbb{B}}_{mk}(s)$ are given in Appendix B. The final step assumes the summation of expressions (11) and (12) for the viscoelastic fields over all points n in accordance with (34) for each moment of time t.

The stresses and strains in the time domain are uniquely expressed via potentials (13)–(16). However, the displacements in the time domain are defined up to some additional terms that could be found after the rigid body motion is fixed, as in [Mogilevskaya et al. 2008].

Error analysis. Three sources of errors can be identified in the present method:

 (i) the error due to the use of the truncated series in the approximations (19) and (21),

 (ii) the error related to the iterative solution of system (27), and

(iii) the error due to the use of the numerical inversion of the Laplace transform.

Error (i) can be effectively controlled by using an appropriate number M_k of Fourier terms for the approximations of the displacements and tractions at k-th circular boundary. The value of M_k for this boundary must be determined in the numerical solution process; it depends mostly on the geometry of the problem, and the following procedure is suggested for evaluating it. First, system (27) is solved for

time 0 to find the instantaneous, "elastic" Fourier coefficients. These coefficients are then substituted in the original equation (6), and the normalized difference ε between the left-hand side and the right-hand side of the equation is compared with the predefined accuracy parameter $\varepsilon_{\text{spec}}$. If ε exceeds $\varepsilon_{\text{spec}}$, the number of Fourier terms is increased. The iterations stop when the specified accuracy level is achieved for every circular boundary. The procedure is described in detail in [Mogilevskaya and Crouch 2001].

Error (ii) can be easily controlled by comparing the solution obtained at a current step of iteration with the solution from the previous step. The iterations in the Gauss–Seidel algorithm proceed until the desired degree of accuracy is achieved. In most cases considered in the present work, no more than 30–50 iterations are required for an accuracy around 10^{-8}.

Error (iii) for the Stehfest algorithm of the inversion cannot be controlled automatically, but several indirect means to control it are available:

- The stresses at the boundary of the half-plane obtained numerically by using the present approach can be compared with the prescribed boundary conditions.

- For several linear viscoelastic models (for example, standard solid and Burgers models), the instantaneous ($t = 0$) or large ($t \to \infty$) time response is the same as for the elastic model. Thus, one can compare the solution obtained by the present approach with the solution of the corresponding elastic problem, which sometimes can be found analytically.

- For the problem of an infinite or semi-infinite perforated viscoelastic plane subjected to constant loading, the stresses in the matrix do not depend on time and are exactly the same as those for the corresponding elastic problem [Huang et al. 2006b; Pyatigorets et al. 2008]. Thus, one may consider the problem in which the inhomogeneities have very small shear moduli so they can simulate the holes in the numerical analysis. The stresses obtained from the solution of this problem should be the same or very close to the stresses obtained from the corresponding elastic problem.

- The viscoelastic stresses, displacements, and strains obtained using the present approach should be consistent with each other. For example, the strains at any time moment can be obtained via transformed Kolosov–Muskhelishvili potentials; see (11) and (12). At the same time, it is easy to find the horizontal strains along a horizontal path or the vertical strains along a vertical path by numerically differentiating the corresponding displacements. In addition, the time-dependent strains inside the elastic inhomogeneities can be found from the stresses by using Hooke's law. The strains found by using both approaches should be in good agreement with each other.

- The comparison of the selected examples with the finite element analysis can provide an idea about the accuracy of the method and the accuracy of the inverse Laplace transform depending on the number of terms in (34).

An extensive study of the accuracy of the numerical inverse Laplace transform was conducted using the means listed above. It was found that for the case of constant loading and for the constitutive models presented in the next section, the best accuracy is achieved when N_{St} ranges from 8 to 10. However, a smaller number of terms in the Stehfest algorithm should be used ($N_{\text{St}} = 4$ to 6) for the calculation of the stresses near the singular points (where the stresses may be subjected to rapid variations). In such cases, the use of a large number N_{St} may cause the sum in (34) to diverge [Stehfest 1970; Cheng et al. 1994]. This effect is usually observed at small times only, and the error introduced by the reduction of the number of terms in (34) is relatively small. See Section 5.1 for some details.

Time-dependent loading is not considered in the present work. For this case the Stehfest algorithm does not provide accurate results. However, the method described in the present paper is not restricted by the use of any particular procedure in the numerical inversion of the Laplace transform.

5. Examples

Two constitutive models for the material matrix are considered in the following numerical examples. The condition of plane strain is assumed hereafter.

For model I it is assumed that the material of the matrix responds as a standard solid (Boltzmann viscoelastic model) in shear (Figure 2, left), and elastically in bulk. Such behavior is quite realistic as the shear modulus for many polymeric solids relaxes much more than its bulk modulus. The constitutive equations for the model are

$$\frac{E_1+E_2}{E_1}\sigma_{ij}(t) + \frac{\eta}{E_1}\dot{\sigma}_{ij}(t) = 2E_2\varepsilon_{ij}(t) + 2\eta\dot{\varepsilon}_{ij}(t), \quad i \neq j \qquad \text{and} \qquad \sigma_{kk}(t) = 3K\varepsilon_{kk}(t), \qquad (36)$$

where σ_{ij} and ε_{ij}, $i \neq j$, are the deviatoric stress and strain, σ_{kk} and ε_{kk} are the volumetric stress and strain, E_1 and E_2 are the elastic moduli of the springs (Figure 2, left), η is the viscosity of the dashpot, K is bulk modulus, and the dot denotes the time derivative. The s-varying analogs of the shear modulus and Kolosov–Muskhelishvili constant are obtained from the procedure described by Wang and Crouch [1982]. They are

$$\hat{\mu}(s) = \frac{E_1(E_2 + \eta s)}{E_1 + E_2 + \eta s}, \qquad \hat{\kappa}(s) = 1 + \frac{6E_1(E_2 + \eta s)}{E_1(E_2 + \eta s) + 3K(E_1 + E_2 + \eta s)}. \qquad (37)$$

For the sake of simplicity, the following values for the material parameters of the viscoelastic matrix are used for all the examples described by the first constitutive model:

$$E_1 = 8 \times 10^3\sigma_0, \quad E_2 = 2 \times 10^3\sigma_0, \quad \eta = 5 \times 10^3\sigma_0 \cdot \text{sec}, \quad K = 17333.3\sigma_0. \qquad (38)$$

The constant σ_0 serves to normalize all the loads and stresses. All elastic moduli can also be expressed via this parameter.

Model II assumes that the bulk material of the viscoelastic matrix behaves according to Burgers model (Figure 2, right) in shear and elastically in bulk. The constitutive equations for this model are

$$\ddot{\sigma}_{ij}(t) + \left(\frac{E_1}{\eta_1} + \frac{E_1}{\eta_2} + \frac{E_2}{\eta_2}\right)\dot{\sigma}_{ij}(t) + \frac{E_1E_2}{\eta_1\eta_2}\sigma_{ij}(t) = 2E_2\ddot{\varepsilon}_{ij}(t) + 2\frac{E_1E_2}{\eta_2}\dot{\varepsilon}_{ij}(t), \qquad i \neq j,$$

$$\sigma_{kk}(t) = 3K\varepsilon_{kk}(t). \qquad (39)$$

Figure 2, right, explains the meanings of the parameters involved in (39). The expressions for the s-varying shear modulus and the Kolosov–Muskhelishvili parameter can be obtained after applying the
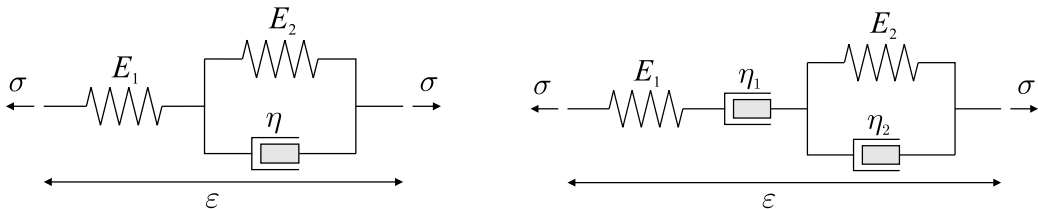

Figure 2. Left: the Boltzmann model. Right: the Burgers model.

Laplace transform to expressions (39). They are

$$\hat{\mu}(s) = \frac{E_1 s \left(s + \frac{E_2}{\eta_2}\right)}{s^2 + s\left(\frac{E_1}{\eta_1} + \frac{E_1}{\eta_2} + \frac{E_2}{\eta_2}\right) + \frac{E_1 E_2}{\eta_1 \eta_2}},$$

$$\hat{\kappa}(s) = 1 + \frac{6E_1 s \left(s + \frac{E_2}{\eta_2}\right)}{E_1 s^2 + \frac{E_1 E_2}{\eta_2} s + 3K\left[s^2 + s\left(\frac{E_1}{\eta_1} + \frac{E_1}{\eta_2} + \frac{E_2}{\eta_2}\right) + \frac{E_1 E_2}{\eta_1 \eta_2}\right]}.$$

(40)

The parameters of the springs and the bulk modulus are taken to be the same as for the first model, and the viscosities of the dashpots are $\eta_1 = 7 \times 10^3 \sigma_0 \cdot \sec$ and $\eta_2 = \eta$; see (38).

It is worth noting that the Poisson's ratio $\nu(t)$ of the viscoelastic matrix is time-dependent for both constitutive models.

In all the examples presented below it is assumed that the loads applied to the boundaries of half-plane do not vary in time. Thus, the functions in (1) are taken as $f_\infty(t) = 1$, $f_p(t) = 1$, $f_F(t) = 1$, the Laplace transform of which gives

$$\hat{f}_\infty(s) = \frac{1}{s}, \quad \hat{f}_p(s) = \frac{1}{s}, \quad \hat{f}_F(s) = \frac{1}{s}.$$

(41)

5.1. *Verification with finite element software ANSYS (model I).* Consider the problem of a viscoelastic half-plane containing two holes and one rigid inhomogeneity as shown in Figure 3. The problem is solved using the present approach and the finite element software ANSYS.

A rectangular domain of size $600R_1 \times 500R_1$ (width × height) is used for the finite element analysis. In order to achieve a high degree of accuracy, the rigid disc is meshed with approximately 23100 quadrilateral 8-node elements, while 131400 elements of the same type are used for the viscoelastic matrix.
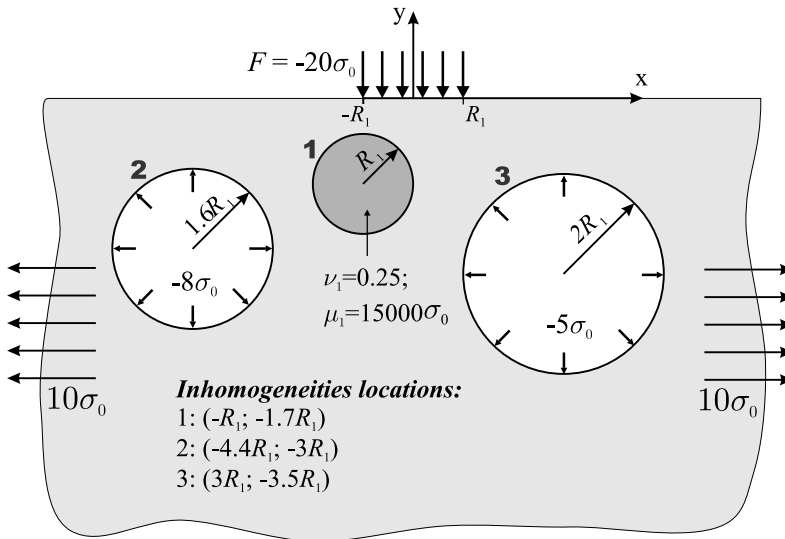

Figure 3. Problem geometry for Example 1.

The use of such a large number of elements is not dictated by any factor; possibly a smaller number of elements can be used to achieve satisfactory accuracy in the results (however, it was found that the use of a mesh with a total of about 35000 elements results in a significantly less accurate solution). The Prony series is adopted to approximate the relaxation of the shear modulus of the matrix. A time stepping algorithm is applied to obtain the time domain solution from the time $t = 0$ till time $t = 10$ sec with time step $\delta t = 0.5$ sec.

The stresses and strains obtained by both approaches can be compared directly. To compare the displacements it is necessary to introduce proper constraints in the finite element model and to constrain rigid body motion in the present approach. The procedure is described in detail in [Pyatigorets et al. 2008].

In the present method, the accuracy parameter $\varepsilon_{\text{spec}}$ is specified at the level $\varepsilon_{\text{spec}} = 10^{-5}$. The number of Fourier terms M_k used in the approximation of the boundary displacements is as follows:

	Left hole	Elastic disc	Right hole
$M_k =$	18	23	20

Using ten terms in sum (34) provides quite accurate results for the numerical Laplace inversion. The calculations with the present method take 8–10 seconds on a Dell computer workstation (Intel P4 3.6 GHz, 2 GB RAM), while the finite element calculations require about 7 hours at the same computer workstation (no special optimization technique is used).

Some illustrative examples are given in Figures 4–7. Figures 4 and 5 show very good agreement between the results for the displacements and strains calculated with both approaches. The graphs in Figures 4 and 5 are plotted for several time instances only (0, 8, and 10 sec), however, good agreement is found for all time moments for which the solution is found. The comparison of the time-dependent stresses, obtained by the present approach for two values of $N_{\text{St}} = 10$ and $N_{\text{St}} = 2$, with the results from the finite element analysis is illustrated in Figures 6 and 7. One can see that for $N_{\text{St}} = 10$, the stresses exhibit very good agreement with those obtained by ANSYS (see Figure 6). For the case of $N_{\text{St}} = 2$ some discrepancy in the results given in Figure 7 is observed at small time values only; at larger time the error reduces greatly. Similar behavior is observed for all the examples considered in the paper. As the discrepancy is sufficiently small it seems reasonable to use a smaller number of terms in the Stehfest algorithm when large N_{St} causes the sum (34) to diverge.

The same procedure was performed to compare the viscoelastic fields for the case of a point force and a force distributed over the whole boundary of the half-plane. The results for these cases also reveal good agreement with the results from the finite element analysis.

5.2. *Example with a single inhomogeneity (model I).* Consider a viscoelastic half-plane containing a single inhomogeneity. The material properties of the half-plane are described by constitutive model I. Four types of loading conditions are considered:

(i) a far-field stress $\sigma^\infty = \sigma_0$ acting parallel to the boundary of the half-plane;

(ii) a point force $F = -\sigma_0$ acting perpendicular to the boundary of the half-plane along the axis of symmetry;

(iii) a force $F = -\sigma_0$ acting perpendicular to the boundary of the half-plane and distributed over the interval of length $2R$ whose center is located on the axis of symmetry;
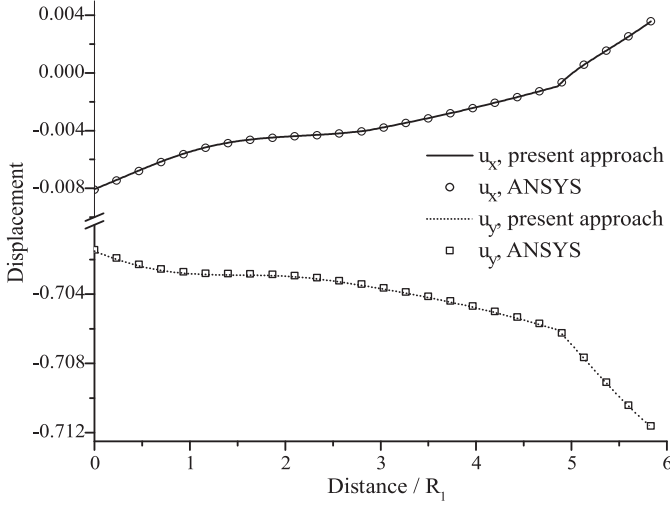
Figure 4. Variation of the displacements along the path $(-3R_1, -5R_1) \div (0, 0)$ at time $t = 8$ sec.
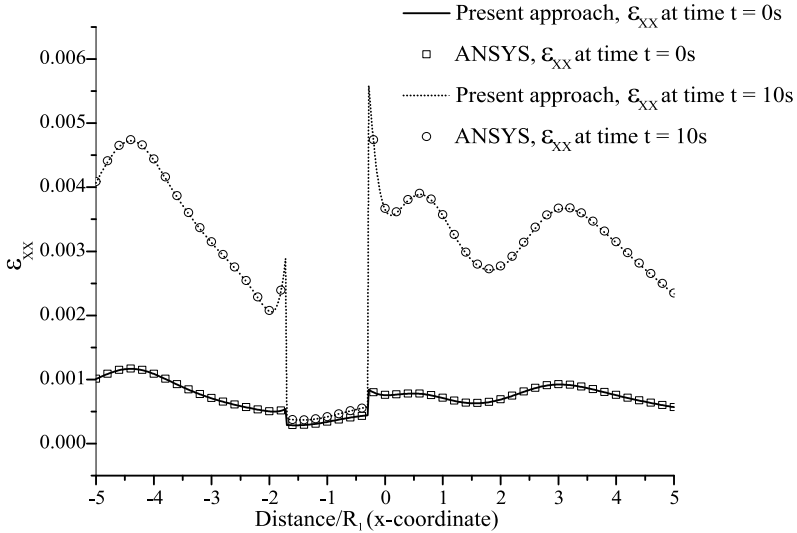

Figure 5. Variation of the horizontal strain along the path $(-5R_1, -R_1) \div (5R_1, -R_1)$.

(iv) a normal force $F = -\sigma_0$ uniformly distributed over the whole boundary of the half-plane.

In this example we study the influence of the shear modulus of the inhomogeneity on the hoop stress at point A (the closest point to the boundary of the half-plane that is located on the intersection of the boundary of the inhomogeneity and the axis of symmetry).

The Poisson's ratio of elastic inhomogeneity is set to $v = 0.35$, while the shear modulus is varied from $\mu_{\text{inh}} = 10^{-3}\sigma_0$ to $\mu_{\text{inh}} = 8 \cdot 10^5 \sigma_0$. It is convenient to normalize μ_{inh} by the instantaneous shear modulus of the viscoelastic matrix $\mu|_{t=0} = 8000\sigma_0$. This value is equal to the elastic modulus E_1 in constitutive model I, as the dashpot does not exhibit instantaneous deformation (see Figure 2, left). Ten terms are
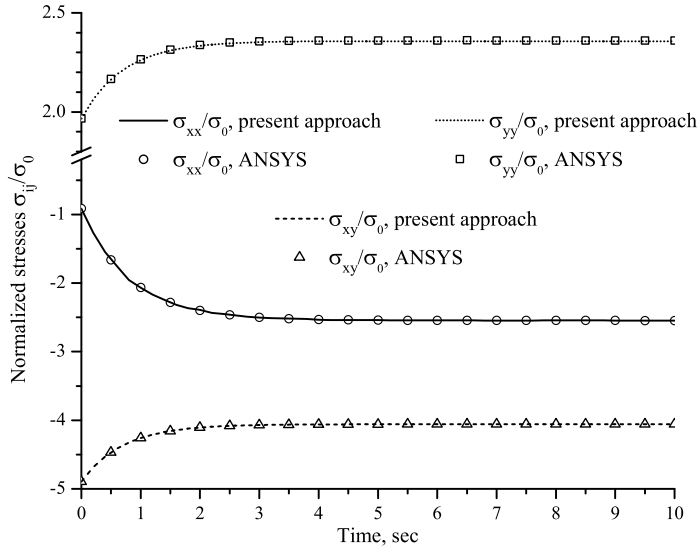
Figure 6. Variation of the normalized stresses at the point $(-2.28R_1, -2.3R_1)$ located inside the viscoelastic matrix ($N_{St} = 10$).
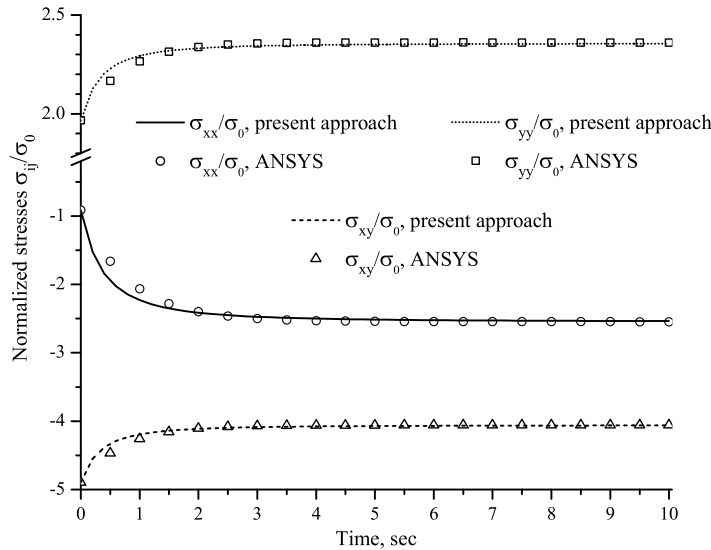

Figure 7. Variation of the normalized stresses at the point $(-2.28R_1, -2.3R_1)$ located in the viscoelastic matrix ($N_{St} = 2$).

used in the procedure of numerical inversion of the Laplace transform, (34), and the number of Fourier terms M_k required to achieve the accuracy level $\varepsilon_{spec} = 10^{-5}$ is the following:

Type of load	Far-field stress	Concentrated force	Force over a segment	Force over the boundary
M_k	37	209	34	22

The fact that the hoop stress at point A is equal to the stress $\sigma_{xx}(t)$ allows for additional verification of the method and the computer code. Consider the case when the shear modulus of the inhomogeneity is close to zero and far-field stress is applied parallel to the boundary of the half-plane. For the inhomogeneity located far away from the boundary of the half-plane, the stresses in the vicinity of the inhomogeneity will not be affected by that boundary and will be the same as in the case of a full plane. In addition, the stresses for this case do not depend on time, and are exactly the same as the stresses in the corresponding "elastic" problem: $\sigma_{xx}/\sigma^{\infty} = 3$. The hoop stress found by the present method for $\mu_{\text{inh}} = 10^{-3}\sigma_0$ and $z_{\text{center}} = (0, -2000R)$ agrees with the elastic solution up to 6 significant digits for any moment in time.

The variation of hoop stress at point A versus the shear modulus of the inhomogeneity is shown in Figures 8–11 for all types of loading. The plots reveal that the hoop stresses vary greatly with the variation of the shear modulus of the inhomogeneity. However, in all four cases, the hoop stresses exhibit an asymptotic behavior when $\mu_{\text{inh}}/\mu \to 0$ (the case of a hole) or $\mu_{\text{inh}}/\mu \to \infty$ (the case of a stiff inhomogeneity). In case (i), the hoop stress is tensile (Figure 8), while in case (iv) it is compressive (Figure 11). The hoop stress changes sign for two remaining cases of loading (Figures 9 and 10).

The hoop stress at point A depends greatly on the separation distance between the inhomogeneity and the boundary of the half-plane. The investigation of this dependency for the case of a hole located in a viscoelastic half-plane is given in [Pyatigorets et al. 2008]. It is interesting to compare the results obtained by the present approach with the results presented in the latter paper. It has been found that the hoop stresses obtained by the present method for $\mu_{\text{inh}} = 10^{-3}\sigma_0$ match with the results provided by Pyatigorets et al. [2008] up to the third decimal number for any moment in time.

5.3. *Example with two inhomogeneities (model II).* Two inhomogeneities with different elastic properties are considered in this example. The geometry of the problem is shown in Figure 12. Both inhomogeneities have the same radii R and their centers are located on the same horizontal line $y = -1.4R$.
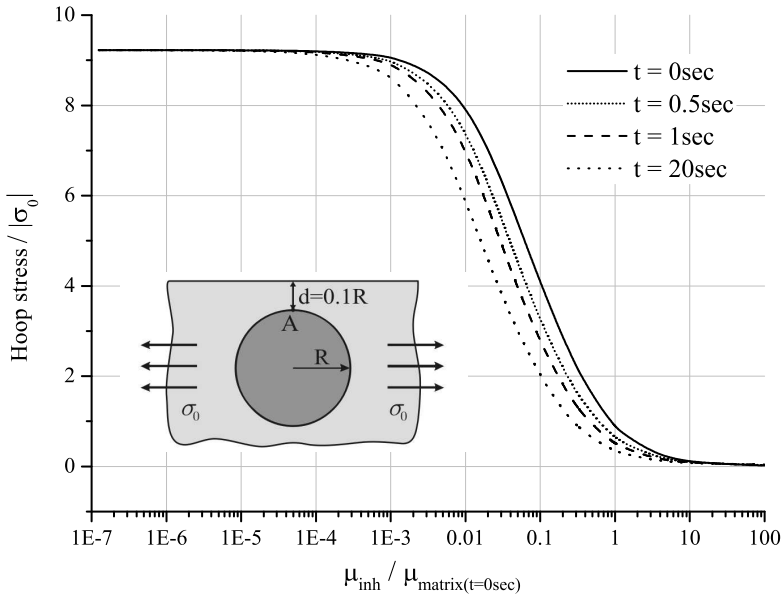

Figure 8. Variation of the normalized hoop stress at point A for loading case (i).
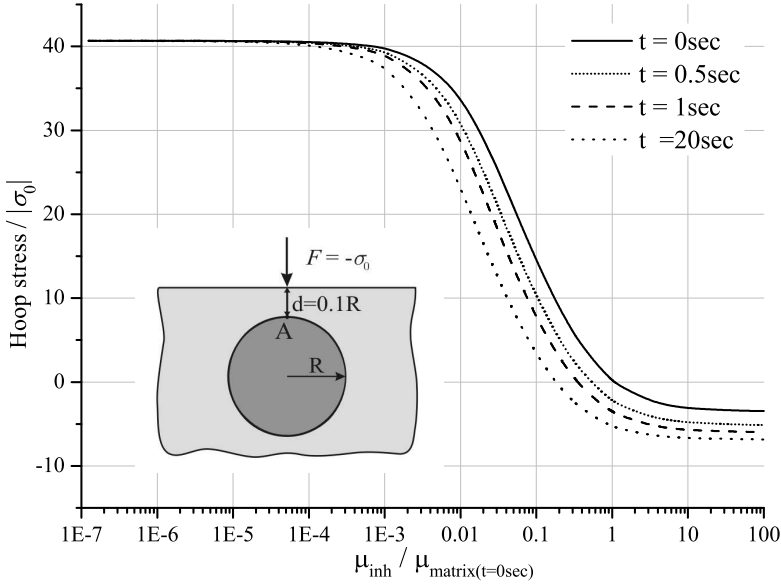
Figure 9. Variation of the normalized hoop stress at point *A* for loading case (ii).
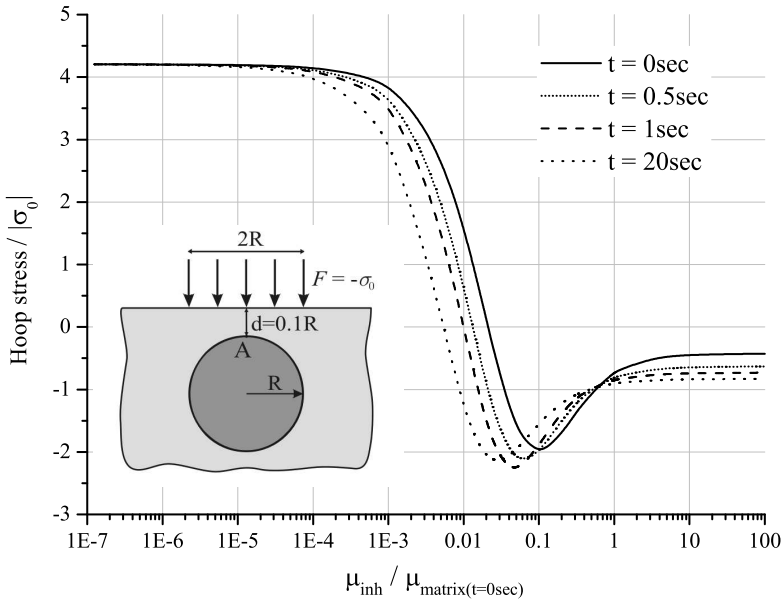

Figure 10. Variation of the normalized hoop stress at point *A* for loading case (iii).

The separation distance between the inhomogeneities is $0.4R$. The far-field stress σ_0 acts parallel to the boundary of the half-plane. The bulk material of the half-plane behaves according to constitutive model II. The properties of the elastic inhomogeneities are as follows:

- Left inhomogeneity: $\nu = 0.35$, $\mu = 32000\sigma_0$ (very rigid inhomogeneity);
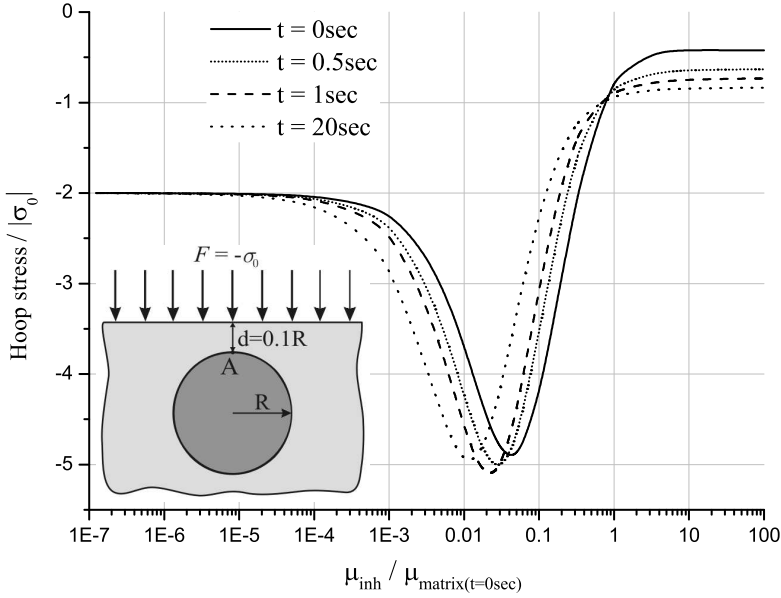- Right inhomogeneity: $\nu = 0.35$, $\mu = 400\sigma_0$ (very soft inhomogeneity).

Figure 11. Variation of the normalized hoop stress at point A for loading case (iv).

The distribution of maximum shear stresses is found for different moments in time. The maximum shear stress at a point is given by the expression

$$\tau_{\max}(z, t) = \tfrac{1}{2}\big(\sigma_1(z, t) - \sigma_2(z, t)\big),$$

where $\sigma_1(z, t)$ is the major in-plane principal stress and $\sigma_2(z, t)$ is the minor in-plane principal stress. The location of maximum shear stress can provide valuable information about the initiation and propagation of cracks.

The accuracy parameter $\varepsilon_{\text{spec}}$ is set to 10^{-5}. To achieve this accuracy 51 terms in Fourier series ($M_k = 25$) are required for each inhomogeneity. The number of terms N_{St} used in the algorithm for the numerical inverse Laplace transform is set to 8. It was found that when one uses 10 terms in approximation (34), the results of the approximation begin to diverge at certain points of the space domain. For additional verification of the results obtained in this example a finite element model was built. The solution found using our approach (for $N_{\text{St}} = 8$) shows very good agreement with the one obtained via finite elements.
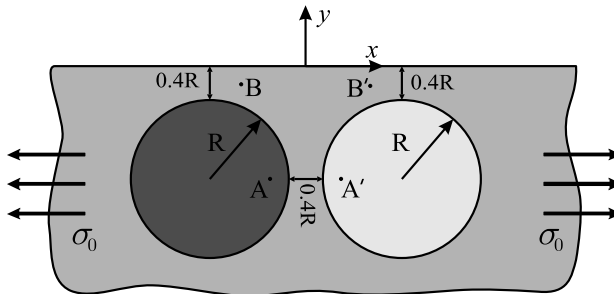

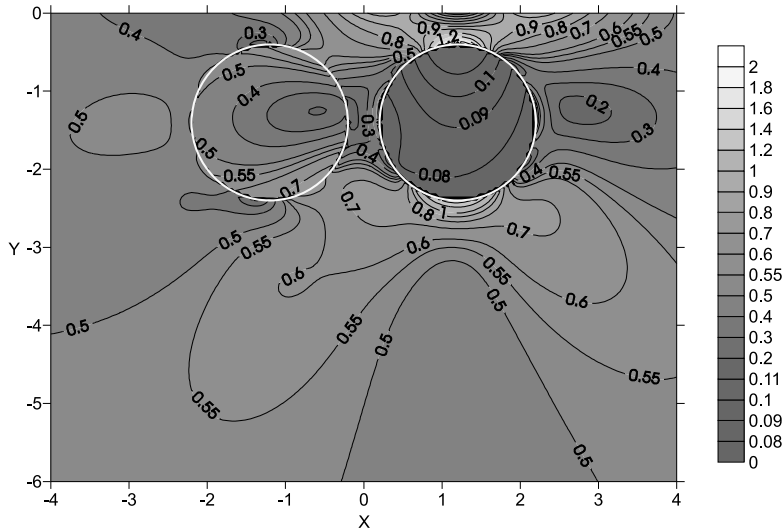**Figure 12.** Problem geometry for Example 3.

Figure 13. Contours of $\tau_{\max}(z, t)/\sigma_0$ at time $t = 0$ sec.
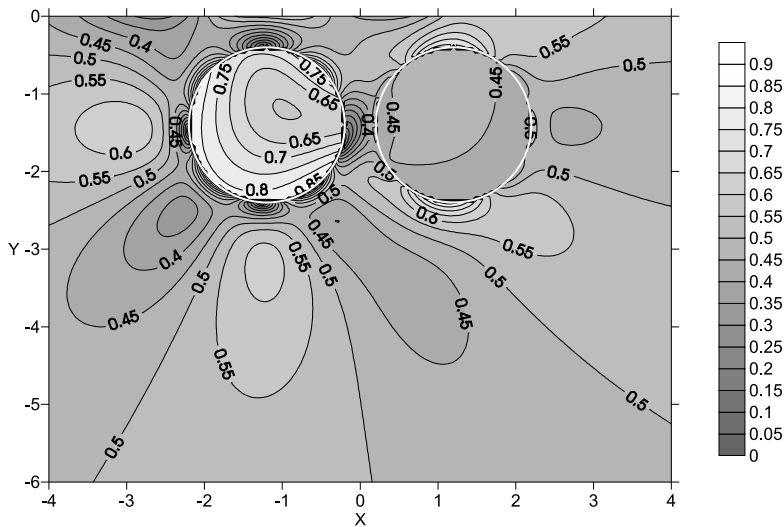

Figure 14. Contours of $\tau_{\max}(z, t)/\sigma_0$ at time $t = 5$ sec.

The contour plots of $\tau_{\max}(z, t)/\sigma_0$ are given in the next three figures for three moments in time: $t = 0$ sec, $t = 5$ sec, and $t = 300$ sec. At the start (Figure 13), the highest shear stress concentration is seen to be localized between the soft inhomogeneity and the boundary of the half-plane. At the same time the stresses inside the inhomogeneity are much lower than in the surrounding bulk material. These results are expected as the distribution of stresses is similar to the one observed for the problem of the perforated half-plane. The stresses inside the stiff inhomogeneity are about the same magnitude as in the surrounding matrix. The next snapshot (Figure 14) reveals that stresses inside the inhomogeneities increase rapidly approaching the magnitude of the far-field stress σ_0 inside the stiff inhomogeneity. The distribution of the stresses in the matrix also changes considerably, but the maximum magnitude of $\tau_{\max}$
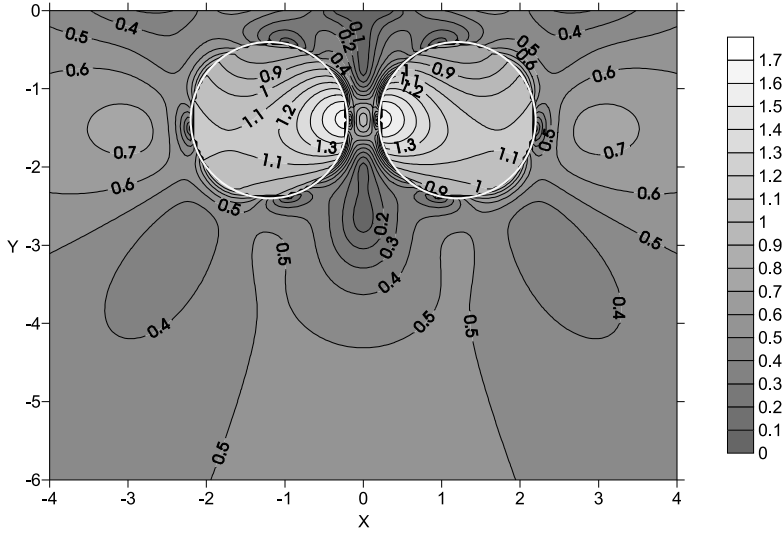
Figure 15. Contours of $\tau_{\max}(z, t)/\sigma_0$ at time $t = 300$ sec.

decreases from the level of $2\sigma_0$ to the level of σ_0. The distribution of stresses at large times (exemplified by Figure 15) becomes symmetric relative to the line $x = 0$. At time $t = 300$ sec the magnitude of the maximum shear stress almost reaches the level of $2\sigma_0$ again, but the maximum stresses are localized inside the inhomogeneities.

The symmetric distribution of maximum shear stresses observed at large times (despite the fact that the material properties of the inhomogeneities are very different) allows one to suggest that for the case of constitutive model II and constant loading, the stresses at large times do not depend on the material properties of the viscoelastic matrix and elastic inhomogeneities. To support this conclusion, stress components are found at a number of points inside the half-plane for several different sets of material properties of the matrix and inhomogeneites. The illustrative results for the case of vertical stress σ_{yy} are presented in Figures 16 and 17. The first set of material properties corresponds to that stated above in the current example. The second set is

$$E_1 = 1000\sigma_0, \quad E_2 = 6000\sigma_0, \quad \eta_1 = 3000\sigma_0 \cdot \text{sec}, \quad \eta_2 = 9000\sigma_0 \cdot \text{sec}, \quad K = 24999\sigma_0,$$

Left inhomogeneity: $\nu = 0.4, \mu = 1200\sigma_0,$

Right inhomogeneity: $\nu = 0.2, \mu = 16000\sigma_0.$

The stresses are found at the points $A = (-0.4R, -1.4R)$ and $A' = (0.4R, -1.4R)$ located inside the left and right inhomogeneities, respectively, and at the points $B = (-0.8R, -0.2R)$ and $B' = (0.8R, -0.2R)$ located inside the matrix. The results, presented in Figures 16 and 17, reveal that the stresses at large times, indeed, do not depend on the material properties, although they depend on the geometry of the problem and on the loading, meaning stresses are statically determined. Similar behavior of stresses is observed for other types of loading considered in the present paper. As a hole can be treated as inhomogeneity with zero elastic properties the same conclusion can be made for the case of more complicated geometries including multiple holes and elastic inhomogeneities. We emphasize that the strains and
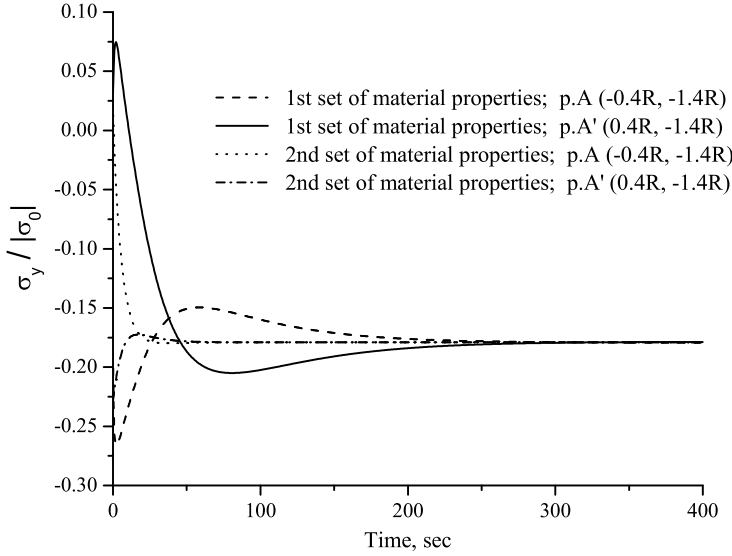
Figure 16. Variation of the normalized vertical stress at points A and A'.
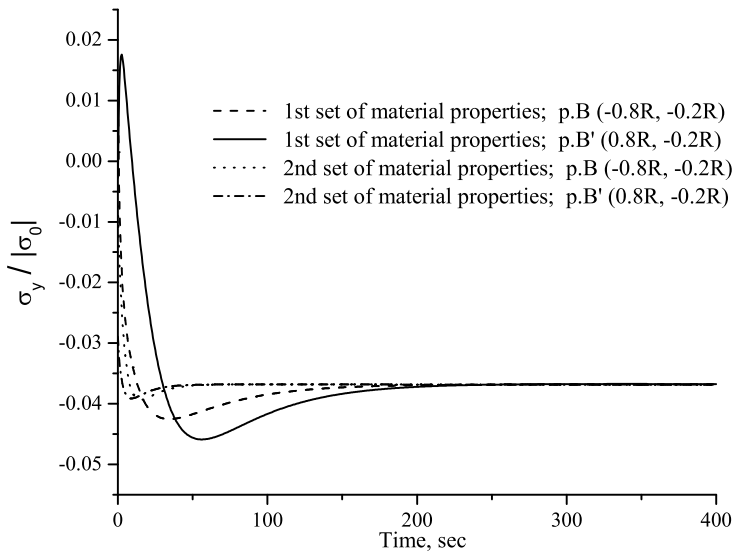

Figure 17. Variation of the normalized vertical stress at points B and B'.

displacements depend on the material properties even when time is large. These results are supported by the results from the finite element analysis.

Note that the numerical analysis for the case when the viscoelastic matrix is described by constitutive model I reveals that the stresses do not exhibit asymptotic behavior at large times. It is the viscous flow introduced by the combination of dashpots in the Burger model that is responsible for the steady solution at large times.

5.4. *Asymptotic behavior at large times (model II).*   In some cases, it is possible to find analytically the behavior of the time-dependent stresses at large times. To illustrate this, we consider the case of a single inhomogeneity in the full plane. For this problem system (6) reduces to the single equation

$$
-2\int_L \frac{\hat{u}^h(\tau;s)}{(\tau-\xi)^2}d\tau + \int_L \hat{u}^h(\tau;s)\frac{\partial^2 K_1(\tau,\xi)}{\partial\tau\partial\xi}d\tau + \int_L \overline{\hat{u}^h(\tau;s)}\frac{\partial^2 K_2(\tau,\xi)}{\partial\bar\tau\partial\xi}d\bar\tau
$$

$$
+\frac{\hat\kappa(s)}{2\hat\mu(s)}\left[\int_L \hat\sigma^h(\tau;s)\frac{\partial K_1(\tau,\xi)}{\partial\xi}d\tau - \int_L \overline{\hat\sigma^h(\tau;s)}\frac{\partial K_2(\tau,\xi)}{\partial\xi}d\bar\tau\right]
$$

$$
+\frac{\hat\kappa(s)-1}{2\hat\mu(s)}\int_L \frac{\hat\sigma^h(\tau;s)}{\tau-\xi}d\tau + \pi i\frac{\hat\kappa(s)+1}{2\hat\mu(s)}\hat\sigma^h(\xi;s) = 2\pi i\frac{\hat\kappa(s)+1}{4\hat\mu(s)}\big(1+g^2(\xi)\big)\hat\sigma^\infty(s), \quad (42)
$$

where L is the boundary of the hole occupied by the inhomogeneity. As there are only two terms $g^0(\xi)\equiv 1$ and $g^2(\xi)$ on the right-hand side of Equation (42), the only nonzero Fourier coefficients $\hat{B}_m(s)$ present in approximations (19) are $\hat{B}_{-1}(s)$ and $\hat{B}_1(s)$. These coefficients are found from the solution of (42) and can be expressed as

$$
\hat{B}_{-1}(s) = \frac{\hat\sigma^\infty(s)}{4}\frac{\hat\kappa(s)+1}{\hat\mu(s)+\hat\kappa(s)\mu_d}R, \qquad \mathrm{Re}\,\hat{B}_1(s) = \frac{\hat\sigma^\infty(s)}{8}\frac{\hat\kappa(s)+1}{\hat\mu(s)+2\mu_d/(\kappa_d-1)}R, \qquad (43)
$$

where R is the radius of the inhomogeneity, and μ_d and κ_d are its shear modulus and Kolosov–Muskhelishvili parameter, respectively.

As an illustration, we investigate the behavior of the Kolosov–Muskhelishvili potential $\varphi(z,t)$ at $t\to\infty$. It follows from (15) that

$$
\hat\varphi(z,s) = -\frac{\mu_d-\hat\mu(s)}{\hat\mu(s)+\hat\kappa(s)\mu_d}\frac{R^2}{z-z_c}\frac{\hat\sigma^\infty(s)}{2} + \frac{\hat\sigma^\infty(s)}{4}z, \qquad z\in\text{matrix},
$$

$$
\hat\varphi(z,s) = \frac{\mu_d}{\kappa_d-1}\frac{\hat\kappa(s)+1}{\hat\mu(s)+2\mu_d/(\kappa_d-1)}(z-z_c)\frac{\hat\sigma^\infty(s)}{4}, \qquad z\in\text{elastic disc},
$$

$$(44)$$

where z_c is the complex coordinate of the center of the inhomogeneity.

The behavior of the potential in the time domain at the time $t\to\infty$ corresponds to the behavior of its Laplace transform at $s\to 0$. Equations (40) give

$$
\hat\mu(s)\to 0, \quad \hat\kappa(s)\to 1 \quad \text{when} \quad s\to 0. \tag{45}
$$

Using (44) and (45) and not accounting for the behavior of $\hat\sigma_{xx}^\infty(s)$ at $s\to 0$ (this quantity should be transformed back in the time domain), we get

$$
\hat\varphi(z,s) = \frac{\hat\sigma^\infty(s)}{4}\left[z-\frac{2R^2}{z-z_c}\right], \qquad z\in\text{matrix}, \qquad s\to 0,
$$

$$
\hat\varphi(z,s) = (z-z_c)\frac{\hat\sigma^\infty(s)}{4}, \qquad z\in\text{elastic disc}, \quad s\to 0.
$$

$$(46)$$

Angle, deg	$t = 0\,\text{sec}$	$t = 5\,\text{sec}$	$t = 500\,\text{sec}$	Equation (47)
Circular contour located inside the matrix ($r = 1.1R$)				
0	1.359325	2.511734	2.652893	2.652893
15	1.311184	2.3092	2.431448	2.431447
30	1.179662	1.755867	1.826447	1.826446
45	0.99999999	1.00000011	1.00000012	1
60	0.820338	0.244133	0.173554	0.173554
75	0.688816	−0.3092	−0.431447	−0.431447
90	0.640676	−0.511733	−0.652893	−0.652893
Circular contour located inside the inhomogeneity ($r = 0.8R$)				
0–360	1.076923	1.006881	1.00000006	1

Table 1. The values of $\sigma_{xx}(z) + \sigma_{yy}(z)$ found numerically and from (47).

Finally using (11) and (46) one arrives at

$$\sigma_{xx}(z) + \sigma_{yy}(z) = \sigma^{\infty}\left[1 + 2\,\text{Re}\left(\frac{R}{z - z_c}\right)^2\right], \qquad z \in \text{matrix}, \qquad t \to \infty,$$

$$\sigma_{xx}(z) + \sigma_{yy}(z) = \sigma^{\infty}, \qquad\qquad\qquad\qquad z \in \text{elastic disc}, \ \ t \to \infty. \tag{47}$$

It follows from expressions (47) that, at large times, the sum of the horizontal and vertical stresses inside the inhomogeneity is constant and equal to the value of the far-field stress. The results given by (47) can be used as the benchmark solution. Consider a single inhomogeneity located far from the boundary of the viscoelastic half-plane subjected to far-field stress σ^{∞}. Let $R = 1$ and $z_c = (5R, -2000R)$. We assume that the viscoelastic matrix obeys constitutive model II, $\nu_d = 0.2$, and $\mu_d = 16000\sigma^{\infty}$. Table 1 shows the results for the combination $\sigma_{xx}(z) + \sigma_{yy}(z)$ calculated at several points located on two circular contours cocentrical with the boundary of the inhomogeneity. The first contour is located inside the inhomogeneity and its radius is $r = 0.8R$; the radius of the contour located outside the inhomogeneity is $r = 1.1R$. For both contours the angle is defined similarly to the angle shown in Figure 1b. Due to the symmetry of the problem the values of $\sigma_{xx}(z) + \sigma_{yy}(z)$ are given for the first quarter of the complex plane only. As one can see from Table 1, the combination $\sigma_{xx}(z) + \sigma_{yy}(z)$ tends to the results prescribed by (47) when time is sufficiently large.

6. Conclusion

We have shown that the proposed method of solution of the problem of a semi-infinite, isotropic, linear viscoelastic half-plane containing multiple, nonoverlapping circular inhomogeneities is efficient and accurate. As the upper boundary of the half-plane may be subjected to different loading conditions, the method can be successfully used in the modeling of indentation processes.

An important feature of the algorithm is that most of the derivation, including space integration and the Laplace transform, is performed analytically. In the case of the perforated half-plane, when the method reduces to the one presented in [Pyatigorets et al. 2008], the inversion of the Laplace transform can be

also performed analytically. However, in the general case of the inhomogeneities, it has to be performed numerically.

An algorithm for numerical inversion of the Laplace transform proposed by Stehfest is used in the present work. It is found that for the case of constant boundary conditions and for the constitutive models presented in the paper, the algorithm provides accurate results. The results of the numerical simulations indicate that the Stehfest algorithm does not provide accurate results for those problems where time-dependent boundary conditions are prescribed. However, the method described in the present paper is not restricted by the use of any particular procedure for the numerical inversion of the Laplace transform.

The major advantage of the algorithm is its time efficiency: problems containing large arrays of inhomogeneities (tens/hundreds) can be accurately solved in a relatively small time on a standard single-processor PC (seconds or minutes if the solution is found at a few spatial points and several hours if the number of points is tens or hundreds of thousands). The calculation of viscoelastic fields can be effectively parallelized on multiprocessor/multicore machines. A multithreading architecture is implemented in the current version of the computer code that allows one to additionally speed up calculations on multiprocessor machines. The present method allows one to easily modify constitutive viscoelastic models in the computer code if the expressions for the transformed shear modulus and the Kolosov–Muskhelishvili parameter are known.

Several numerical examples are considered in the paper. Interesting results are obtained from the study of the hoop stress at a point on the boundary of a single inhomogeneity located in the vicinity of the boundary of the half-plane. The study reveals that the hoop stress greatly depends on the material properties of the inhomogeneity and can be tensile or compressive depending on the time moment and shear modulus of the inhomogeneity. The results obtained for constitutive model II (Example 3) show that the state of the stresses is statically determined at large times, with an asymptotic behavior as $t \to \infty$ determined only by the geometry of the problem. Nevertheless, the value of t when the stresses approach the asymptotic behavior depends on the material parameters.

One of the future developments of the approach may include the consideration of imperfect interfaces between the inhomogeneities and the matrix. Cracks or inhomogeneities of more general geometry can also be incorporated, although the method would have to employ the boundary element technique.

Appendix A

The operator $\hat{\Lambda}_{kk}$ is the Laplace transform of the corresponding operator presented in [Dejoie et al. 2006]:

$$\hat{\Lambda}_{kk}(\xi; s) = -\frac{1}{R_k}\left\{ 2\,\mathrm{Re}\,\hat{B}_{1k} + \sum_{m=1}^{M_k-1} m\hat{B}_{-mk} g_k^{m+1}(\xi) + \sum_{m=2}^{M_k+1} \hat{B}_{mk} g_k^{1-m}(\xi) \right\}. \tag{A.1}$$

The operator $\hat{G}_{kk}$ is given by

$$\begin{aligned}
\hat{G}_{kk}(\xi; s) &= \frac{1}{R_k}\left\{ 2\left(\frac{\mu_k}{\kappa_k-1}\frac{\hat{\kappa}-1}{\hat{\mu}} - 1\right)\mathrm{Re}\,\hat{B}_{1k} \right. \\
&\qquad \left. + \left(\frac{\mu_k}{\hat{\mu}} - 1\right)\sum_{m=1}^{M_k-1} m\hat{B}_{-mk} g_k^{m+1}(\xi) + \left(\frac{\mu_k}{\kappa_k}\frac{\hat{\kappa}}{\hat{\mu}} - 1\right)\sum_{m=2}^{M_k+1} \hat{B}_{mk} g_k^{1-m}(\xi) \right\} \\
&= -\frac{1}{R_k}\left\{ 2\hat{\alpha}_{2k}\,\mathrm{Re}\,\hat{B}_{1k} + \hat{\alpha}_{1k}\sum_{m=1}^{M_k-1} m\hat{B}_{-mk} g_k^{m+1}(\xi) + \hat{\alpha}_{3k}\sum_{m=2}^{M_k+1} \hat{B}_{mk} g_k^{1-m}(\xi) \right\}. \tag{A.2}
\end{aligned}$$

Expression (A.2) differs from (A.1) by the presence of additional terms in front of unknown Fourier coefficients $\hat{B}_{-mk}$, Re $\hat{B}_{1k}$, and $\hat{B}_{mk}$ only. All other operators $\hat{G}_{jk}$ can be obtained in a similar way from the corresponding expressions given in [Dejoie et al. 2006].

Appendix B

Potentials for the k-th elastic disc derived from (13)*:*

$$\hat{\varphi}(z,s) = \frac{2\mu_k}{\kappa_k - 1} \operatorname{Re} \hat{B}_{1k} g_k^{-1}(z) + \frac{2\mu_k}{\kappa_k} \sum_{m=2}^{M_k+1} \hat{B}_{mk} g_k^{-m}(z)$$

$$= \frac{2\mu_k}{\kappa_k - 1} \frac{1}{\hat{\alpha}_{2k}} \operatorname{Re} \hat{\mathbb{B}}_{1k} g_k^{-1}(z) + \frac{2\mu_k}{\kappa_k} \frac{1}{\hat{\alpha}_{3k}} \sum_{m=2}^{M_k+1} \hat{\mathbb{B}}_{mk} g_k^{-m}(z), \quad \text{(B.1)}$$

$$\hat{\psi}(z,s) = -\frac{2\mu_k}{\kappa_k - 1} \frac{\bar{z}_k}{R_k} \operatorname{Re} \hat{B}_{1k} - \frac{2\mu_k}{\kappa_k} \left[\frac{\bar{z}_k}{R_k} + g_k(z) \right] \sum_{m=2}^{M_k+1} m \hat{B}_{mk} g_k^{-(m-1)}(z) - 2\mu_k \sum_{m=1}^{M_k-1} \overline{\hat{B}_{-mk}} g_k^{-m}(z)$$

$$= -\frac{2\mu_k}{\kappa_k - 1} \frac{\bar{z}_k}{\hat{\alpha}_{2k} R_k} \operatorname{Re} \hat{\mathbb{B}}_{1k}$$

$$- \frac{2\mu_k}{\hat{\alpha}_{3k}\kappa_k} \left[\frac{\bar{z}_k}{R_k} + g_k(z) \right] \sum_{m=2}^{M_k+1} m \hat{\mathbb{B}}_{mk} g_k^{-(m-1)}(z) - \frac{2\mu_k}{\hat{\alpha}_{1k}} \sum_{m=1}^{M_k-1} \overline{\hat{\mathbb{B}}_{-mk}} g_k^{-m}(z). \quad \text{(B.2)}$$

Similar expressions are used in [Mogilevskaya et al. 2008] for the calculation of elastic potentials.

Potentials for the matrix derived from (15) *and* (16)*:*

$$\hat{\varphi}_{\text{plane}}(z;s) = \frac{2\hat{\mu}}{\hat{\kappa}+1} \sum_{k=1}^{N} \sum_{m=1}^{M_k-1} \overline{\hat{\mathbb{B}}_{-mk}} g_k^m(z) + \frac{\hat{\sigma}^{\infty}(s)}{4} z, \quad \text{(B.3)}$$

$$\hat{\psi}_{\text{plane}}(z;s) = -\frac{\hat{\kappa}-1}{\hat{\kappa}+1} \sum_{k=1}^{N_h} \hat{p}_k R_k g_k(z) + \frac{2\hat{\mu}}{\hat{\kappa}+1} \sum_{k=1}^{N} \left[-2 \operatorname{Re} \hat{\mathbb{B}}_{1k} g_k(z) \right.$$

$$\left. + \sum_{m=1}^{M_k-1} m \overline{\hat{\mathbb{B}}_{-mk}} g_k^{m+1}(z) \left(\frac{\bar{z}_k}{R_k} + g_k(z) \right) - \sum_{m=1}^{M_k+1} \overline{\hat{\mathbb{B}}_{mk}} g_k^m(z) \right] - \frac{\hat{\sigma}^{\infty}(s)}{2} z, \quad \text{(B.4)}$$

$$\hat{\varphi}_{\text{aux}}(z;s) = \frac{\hat{\kappa}-1}{\hat{\kappa}+1} \sum_{j=1}^{N_h} \hat{p}_j R_j h_j(z) + \frac{2\hat{\mu}}{\hat{\kappa}+1} \sum_{j=1}^{N} \left[2 \operatorname{Re} \hat{\mathbb{B}}_{1j} h_j(z) \right.$$

$$\left. + \sum_{m=1}^{M_j-1} m \overline{\hat{\mathbb{B}}_{-mj}} h_j^{m+1}(z) \left(g_j^{-1}(z) - h_j(z) \right) + \sum_{m=2}^{M_j+1} \hat{\mathbb{B}}_{mj} h_j^m(z) \right], \quad \text{(B.5)}$$

$$\hat{\psi}_{\text{aux}}(z;s) = \frac{\hat{\kappa}-1}{\hat{\kappa}+1} z \sum_{j=1}^{N_h} \hat{p}_j h_j^2(z) + \frac{2\hat{\mu}}{\hat{\kappa}+1} \frac{z}{R_j} \sum_{j=1}^{N} \left\{ 2 \operatorname{Re} \hat{\mathbb{B}}_{1j} h_j^2(z) + \sum_{m=2}^{M_j+1} m \hat{\mathbb{B}}_{mj} h_j^{m+1}(z) \right.$$

$$\left. - \sum_{m=1}^{M_j-1} m \overline{\hat{\mathbb{B}}_{-mj}} h_j^{m+1}(z) \left[1 - (m+1) g_j^{-1}(z) h_j(z) + (m+2) h_j^2(z) + \frac{1}{m} \frac{R_j}{z} h_j^{-1}(z) \right] \right\}, \quad \text{(B.6)}$$

where

$$h_j(z) = \frac{R_j}{z - \bar{z}_j}. \quad \text{(B.7)}$$

The potentials $\hat{\varphi}_F(z; s)$ and $\hat{\psi}_F(z; s)$ are due to the use of Flamant's fundamental solution, and they do not depend on the displacements or stresses at the boundaries of the holes. The expressions for these potentials are given in [Pyatigorets et al. 2008].

References

[Carini et al. 1991] A. Carini, M. Diligenti, and G. Maier, "Boundary integral equation analysis in linear viscoelasticity: variational and saddle point formulations", *Comput. Mech.* **8**:2 (1991), 87–98.

[Cheng et al. 1994] A. Cheng, P. Sidauruk, and Y. Abousleiman, "Approximate inversion of the Laplace transform", *Math. J.* **4**:2 (1994), 76–82.

[Davies and Martin 1979] B. Davies and B. Martin, "Numerical inversion of the Laplace transform: a survey and comparison of methods", *J. Comput. Phys.* **33**:1 (1979), 1–32.

[Dejoie et al. 2006] A. Dejoie, S. G. Mogilevskaya, and S. L. Crouch, "A boundary integral method for multiple circular holes in an elastic half-plane", *Eng. Anal. Bound. Elem.* **30**:6 (2006), 450–464.

[Findley et al. 1976] W. N. Findley, J. S. Lai, and K. Onaran, *Creep and relaxation of nonlinear viscoelastic materials*, North-Holland Series in Applied Mathematics and Mechanics **18**, North-Holland, Amsterdam, 1976. Reprinted Dover, New York, 1989.

[Huang et al. 2005a] Y. Huang, S. L. Crouch, and S. G. Mogilevskaya, "A time domain direct boundary integral method for a viscoelastic plane with circular holes and elastic inclusions", *Eng. Anal. Bound. Elem.* **29**:7 (2005), 725–737.

[Huang et al. 2005b] Y. Huang, S. L. Crouch, and S. G. Mogilevskaya, "Direct boundary integral procedure for a Boltzmann viscoelastic plane with circular holes and elastic inclusions", *Comput. Mech.* **37**:1 (2005), 110–118.

[Huang et al. 2006a] Y. Huang, S. G. Mogilevskaya, and S. L. Crouch, "Complex variable boundary integral method for linear viscoelasticity, I: Basic formulation", *Eng. Anal. Bound. Elem.* **30**:12 (2006), 1049–1056.

[Huang et al. 2006b] Y. Huang, S. G. Mogilevskaya, and S. L. Crouch, "Semi-analytical solution for a viscoelastic plane containing multiple circular holes", *J. Mech. Mater. Struct.* **1**:3 (2006), 471–501.

[Kaloerov and Mironenko 2007] S. A. Kaloerov and A. B. Mironenko, "Analyzing the viscoelastic state of a plate with elliptic or linear elastic inclusions", *Int. Appl. Mech.* **43**:2 (2007), 198–208.

[Kaminskii et al. 2002] A. A. Kaminskii, N. I. Zatula, and V. N. Dyakon, "Investigation of the stress-strain state of viscoelastic piecewise-homogeneous bodies by the method of boundary integral equations", *Mech. Compos. Mater.* **38**:3 (2002), 209–214.

[Kumar 2000] U. Kumar, "Computer-aided numerical inversion of Laplace transform", *Active and Passive Elec. Comp.* **22**:3 (2000), 189–213.

[Kushch et al. 2006] V. I. Kushch, S. V. Shmegera, and V. A. Buryachenko, "Elastic equilibrium of a half plane containing a finite array of elliptic inclusions", *Int. J. Solids Struct.* **43**:11–12 (2006), 3459–3483.

[Legros et al. 2004] B. Legros, S. G. Mogilevskaya, and S. L. Crouch, "A boundary integral method for multiple circular inclusions in an elastic half-plane", *Eng. Anal. Bound. Elem.* **28**:9 (2004), 1083–1098.

[Melan 1932] E. Melan, "Der Spannungszustand der durch eine Einzelkraft im Innern benaspruchten Halbscheibe", *Z. Angew. Math. Mech.* **12** (1932), 343–346.

[Mogilevskaya 2000] S. G. Mogilevskaya, "Complex hypersingular integral equation for the piece-wise homogeneous half-plane with cracks", *Int. J. Fract.* **102**:2 (2000), 177–204.

[Mogilevskaya and Crouch 2001] S. G. Mogilevskaya and S. L. Crouch, "A Galerkin boundary integral method for multiple circular elastic inclusions", *Int. J. Numer. Methods Eng.* **52**:10 (2001), 1069–1106.

[Mogilevskaya and Linkov 1998] S. G. Mogilevskaya and A. M. Linkov, "Complex fundamental solutions and complex variables boundary element method in elasticity", *Comput. Mech.* **22**:1 (1998), 88–92.

[Mogilevskaya et al. 2008] S. G. Mogilevskaya, S. L. Crouch, and H. K. Stolarski, "Multiple interacting circular nano-inhomogeneities with surface/interface effects", *J. Mech. Phys. Solids* **56**:6 (2008), 2298–2327.

[Muskhelishvili 1959] N. I. Muskhelishvili, *Some basic problems of the mathematical theory of elasticity*, Noordhoff, Groningen, 1959.

[Pyatigorets et al. 2008] A. V. Pyatigorets, S. G. Mogilevskaya, and M. O. Marasteanu, "Linear viscoelastic analysis of a semi-infinite porous medium", *Int. J. Solids Struct.* **45**:5 (2008), 1458–1482.

[Rabotnov 1988] Y. N. Rabotnov, Механика деформируемого твердого тела, Nauka, Moscow, 1988.

[Stehfest 1970] H. Stehfest, "Algorithm 368: Numerical inversion of Laplace transforms", *Commun. ACM* **13**:1 (1970), 47–49.

[Wang and Crouch 1982] Y. Wang and S. L. Crouch, "Boundary element methods for viscoelastic media", Chapter 73, pp. 705–711 in *Issues in rock mechanics: Proceedings of the Twenty-Third Symposium on Rock Mechanics* (Berkeley, CA, 1982), edited by R. E. Goodman and F. E. Heuze, The Society of Mining Engineers of the American Institute of Mining, Metallurgical and Petroleum Engineers, New York, 1982.

[Wang et al. 2003] J. Wang, S. L. Crouch, and S. G. Mogilevskaya, "A complex boundary integral method for multiple circular holes in an infinite plane", *Eng. Anal. Bound. Elem.* **27**:8 (2003), 789–802.

[Zatula and Lavrenyuk 1995] N. I. Zatula and V. I. Lavrenyuk, "Stressed-strained state of a viscous half-plane with circular inclusions", *Int. Appl. Mech.* **31**:9 (1995), 754–760.

ANDREY V. PYATIGORETS: pyati002@umn.edu
*Department of Civil Engineering, University of Minnesota, 500 Pillsbury Drive SE, Minneapolis, MN 55455,
United States*

SOFIA G. MOGILEVSKAYA: mogil003@umn.edu
*Department of Civil Engineering, University of Minnesota, 500 Pillsbury Drive SE, Minneapolis, MN 55455,
United States*
http://www.ce.umn.edu/people/faculty/mogilevs/